Environmental Science Advances

ROYAL SOCIETY OF CHEMISTRY

CRITICAL REVIEW

View Article Online
View Journal | View Issue

Check for updates

Cite this: *Environ. Sci.: Adv.*, 2024, **3**, 983

A review of current developments in graphene oxide–polysulfone derived membranes for water remediation

Muhammad Zubair, [a] Sadia Farooq,[b] Ajaz Hussain,[b] Sadia Riaz[b] and Aman Ullah *[a]

Water pollution has become a major issue due to the presence of hazardous pollutants resulting from ever-increasing industrial growth, and researchers are actively seeking innovative solutions for water treatment. Graphene Oxide (GO)–polysulfone (PSF) membranes are widely used in water remediation due to their resistance to high pH and harsh chemicals, and their ability to remove water pollutants. These materials have unique two-dimensional structures, tailorable micropores, large surface areas, and fascinating surface properties, making them ideal for water treatment. This review article provides a comprehensive overview of the latest developments in polysulfone-derived membranes modified with graphene oxide, including their separation performance, antifouling effect, and ability to separate and degrade organic pollutants. Additionally, the review article covers membrane performance for filtration of organic dyes, metal ions, radionuclides and salts from contaminated water. The review article also highlights simulation or computational studies and concludes by discussing the challenges and prospects of GO–PSF derived membranes for water remediation.

Received 17th February 2024
Accepted 7th May 2024

DOI: 10.1039/d4va00058g

rsc.li/esadvances

Environmental significance

Water pollution poses a significant threat to both the environment and public health, primarily due to unregulated industrial development. Numerous individuals worldwide lack access to clean drinking water, underscoring the need for effective water treatment methods. Membrane technology, which encompasses polymeric membranes, such as polysulfone, demonstrates promise due to its cost-effective nature and mechanical properties. However, further research is essential to explore the use of nanomaterials, such as graphene oxide (GO), to enhance the performance of these membranes. The development of advanced composite membranes holds great potential for addressing water pollution and scarcity, preserving water resources, and promoting sustainable environmental management.

1. Introduction

The escalating population and unprecedented industrialization have imposed numerous challenges, including a hazardous environment, on our generation. The byproducts of industrial processes have permeated the air and water, contaminating water resources and depriving humans and other living organisms of clean water.[1–4] The World Health Organization (WHO) reports that billions of individuals are faced with a shortage of hygienic drinking water.[5] Additionally, oil spills from transportation, drilling, and storage activities further exacerbate the pollution of water resources.[6,7] The need for potable water and a solution for the global water scarcity problem has led to the development of effective water treatment methods.[8,9]

Membrane technology is of considerable importance in the separation process. It is a highly effective method for treating wastewater, effluents, and seawater desalination due to its cost-efficiency, high productivity, exceptional removal efficiency, straightforward operation, and minimal reliance on chemical additives.[10–13] A membrane serves as a physical barrier that allows for selective permeation of desired materials, while preventing the passage of unwanted materials.[10,14] Membranes are classified based on various characteristics, including the material used for their fabrication, the surface properties of the membrane, and the filtration process and pore size.[15] They are typically divided into polymeric and inorganic membranes, which differ in the materials used for their construction. Inorganic membranes are made from metals and ceramic materials and possess high thermal, structural, and mechanical strength. However, they have limited permeability and are therefore less commonly used.[16] The issue of permeability has been addressed through the use of polymeric membranes. Membranes are typically classified based on their surface properties as either hydrophilic (polar surface) or hydrophobic (non-polar surface).

[a]*Department of Agricultural, Food and Nutritional Science, Lab# 540, South Academic Building University of Alberta, Edmonton, Alberta, Canada T6G 2P5. E-mail: ullah2@ualberta.ca*

[b]*Institute of Chemical Sciences, Bahauddin Zakariya University, Multan 60800, Punjab, Pakistan*

Open Access Article. Published on 07 May 2024. Downloaded on 2/16/2026 7:11:56 AM. This article is licensed under a Creative Commons Attribution-NonCommercial 3.0 Unported Licence.

Open Access Article. Published on 07 May 2024. Downloaded on 2/16/2026 7:11:56 AM. This article is licensed under a Creative Commons Attribution-NonCommercial 3.0 Unported Licence.

Additionally, the filtration process and pore size are also used to categorize membranes into Nano-Filtration (NF), Micro-Filtration (MF), Ultra-Filtration (UF), and Reverse Osmosis (RO) membranes.[17–21]

MF membranes have a pore size ranging from 0.1–1 μm, making them suitable for the separation of macromolecules, colloids, and bacteria.[22] UF membranes have a pore size of 0.01–0.1 μm, making them impermeable to viruses and macromolecules, yet permeable to water molecules and low molecular weight solutes.[23] NF membranes have a pore size of 0.1–0.001 μm, making them more dense than MF and UF membranes, and they are capable of removing divalent ions while allowing monovalent ions to pass.[24,25] RO membranes have a pore size of less than 0.001 μm, making them the densest of all membranes, and they are only used in high-pressure filtration processes to produce clean water by removing impurities and monovalent ions.[26,27]

Polymeric materials, such as polysulfones and polyamides, are commonly used membranes.[28,29] Polysulfones are widely employed polymers in water treatment applications due to their porous structure, favorable mechanical properties, relatively low cost, and ease of operation.[30,31] Additionally, they exhibit resistance to higher pH, high temperatures, and chemical inertness. However, the hydrophobic nature of PSF limits its use, as these membranes are prone to fouling.[32,33]

To address this issue, various nanomaterials, including zeolite, MOFs (metal–organic frameworks), metal carbides, chalcogenides, carbon-composite based nanofibers and carbonaceous materials, are suitable for enhancing the characteristics of PSF membranes.[34–39] Graphene derivatives, such as graphene oxide (GO), are the most popular carbonaceous materials used to improve the separation performance of membranes. GO is a well-known graphene derivative and is commonly used for synthesizing composite membranes.[40–42] The addition of GO not only decreases the membrane's hydrophobicity but also improves its mechanical properties. GO has oxygen;[43,44] as a result, the GO surface is electron-rich (negatively charged) and exhibits excellent adsorption of cationic compounds.[45–47] Moreover, these membranes do not swell in water and remain stable.[48,49] Single layer GO nanosheets are two-dimensional and approximately 1–2 nm thick. Due to their high surface area, GO nanosheets exhibit high interaction with PSF membranes.[46,49,50] These extraordinary surface and dimensional properties make GO a promising candidate for the development of PSF composite membranes. These PSF composite materials exhibit extraordinary structural properties, including increased hydrophilicity, high chemical stability, water permeation, and excellent antifouling properties.[51–53]

So, the objective of this review is to examine the most recent advancements made in PSF membranes that have been modified with graphene oxide, specifically their applications for water remediation. This literature review distinguishes itself from prior studies by providing a comprehensive review of graphene oxide–polysulfone based membranes, covering aspects such as performance, mechanism, properties and computational studies, all within a single review article.

2. Methods of preparation of GO and PSF

The utilization of graphene derivatives, particularly those derived from carbonaceous materials, has become increasingly popular for enhancing the performance of membranes utilized for separation purposes. Among these derivatives, graphene oxide (GO) is notably prominent and widely employed in the fabrication of composite membranes.[54] Graphene oxide (GO) has the ability to not only decrease the hydrophobicity of membranes but also enhance their mechanical properties. This is due to the presence of oxygenated groups on the GO surface.[55] The electron-rich (negatively charged) GO surface exhibits an exceptional ability for the adsorption of cationic compounds. This is attributed to the electrostatic repulsive force that repels negatively charged ions from passing through the surface. As illustrated in Fig. 1, the single layer GO nanosheet is two-dimensional with a one atom thickness, translating to approximately 1–2 nm. The high surface area of GO nanosheets facilitates their remarkable interaction with membranes.[3,57] The remarkable surface and dimensional characteristics of GO nanosheets make them a more favourable option for the fabrication of composite membranes. These composite materials exhibit exceptional structural properties, such as elevated hydrophilicity, enhanced chemical stability, superior water permeability, and anti-fouling properties.[54]

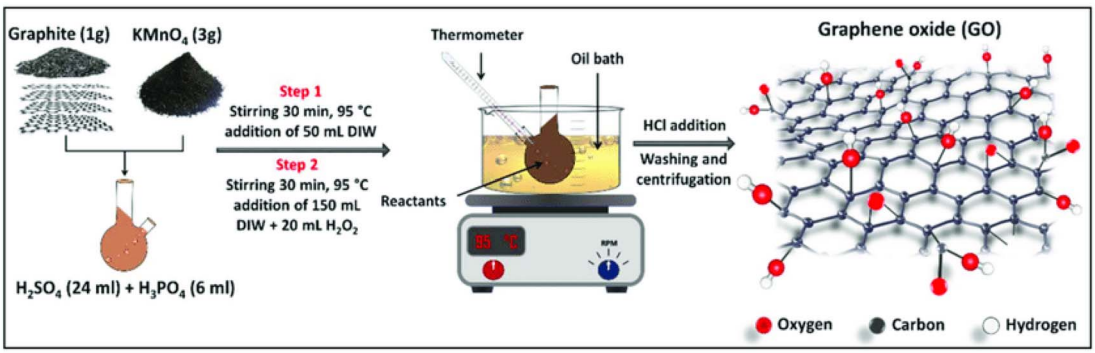

Fig. 1 GO synthesis by a modified Hummer's method.[57]

© 2024 The Author(s). Published by the Royal Society of Chemistry

Open Access Article. Published on 07 May 2024. Downloaded on 2/16/2026 7:11:56 AM. This article is licensed under a Creative Commons Attribution-NonCommercial 3.0 Unported Licence.

There are numerous techniques employed in the production of membranes, including stretching, track-etching, dip-coating, template-leaching, sintering, and phase inversion. Among these methods, phase inversion is the most commonly utilized procedure for generating membranes from polymers.[58–62]

The phase-inversion method (immersion–precipitation technique) is widely used for the generation of membranes from polysulfone like other polymers such as polycarbonates, polyoxadiazoles, polyamides, nylon 6,6, polyphenylene oxide and polyimides.[63–65] This technique consists of four steps: solution preparation of PSF in a suitable solvent, film formation of PSF solution on a flat support, film immersion in a coagulation bath having polymer solvent and conditioning of the membrane.[59,66,67] The schematic procedure of the phase inversion method is shown in Fig. 2.

GO required for the fabrication of the membrane is prepared from the exfoliation of graphite oxide, which is used for cost-effective and large-scale production of GO. Different methods have been reported for the generation of graphite oxide from graphite. Foremost, Brodie prepared graphite oxide by graphite oxidation in a potassium chlorate mixture. After that, Staudenmaier *et al.* reported a method (Staudenmaier method) of graphite oxidation using an ice bath with a 1 : 4 volume ratio of nitric acid : sulphuric acid and potassium chlorate as an oxidizing agent. Then, with continuous stirring, 4.37 g/100 mL graphite was added to an ice bath. Although the evolution of toxic gases is a limitation of the Staudenmaier method, it is considered more secure than the Brodie method. In 1958, Hummer reported another method involving the oxidation of graphite in a few hours using H_2SO_4, $NaNO_3$ and $KMnO_4$ as oxidizing agents. Hummers' Method (HM) has advantages, *i.e.* less reaction time, safety from toxic explosives (ClO_2 and $KClO_3$) because of using $KMnO_4$ instead of $KClO_3$ and removal of acid fog formation using $NaNO_3$ instead of HNO_3. Therefore, HM is preferred over the others for GO preparation. Later on, in 2010, Tour *et al.* further improved HM to enhance the degree of oxidation and to reduce the formation of toxic gases NO_2 and N_2O_4. In the Tour method, $KMnO_4$ replaced sodium nitrate.[69–74] Epoxy is the dominant group in graphene oxide (generated by the Hummer and Tour method). GO synthesis reported by HM has extended sheets and is effective for developing the mechanical properties of membranes. GO has lateral dimensional thickness with amphiphilic nature due to the existence of a variety of surface functionalities and chemical inertness.[75,76]

3. Separation mechanisms

3.1 Classical adsorption

The general adsorption process involving the transfer of materials to the surface of the solid phase, through either physical or chemical interactions, is followed during classical adsorption through membranes. The adsorption of metal ions by a membrane (Fig. 3) consists of three steps. The first step is the penetration along with the diffusion of metal ions through membrane pores and finger-like layers, the 2nd step consists of surface complexation on inner spheres, which are external to nano-sized adsorbents that are localized inside the membrane structure, the third step involves the transfer of metal ions towards the interface of the adsorbent and the last step is the equilibrium stage. The preparation, characterization and adsorptive removal of heavy metal ions from aqueous solution using GO-impregnated membranes have been reported.[77,78]

3.2 Sieving mechanism/size exclusion (steric hindrance)

A particle removal process that prevents particles from passing through any passage/way or pore smaller than the size of the particle itself is called sieving.[79] This process is presented in Fig. 4(a). The membrane can only pass the particles that are smaller than the pore size. Salt ions having hydrated ionic diameters greater than the pore size of the membrane are rejected due to steric hindrance.[80] Uncharged or neutral solutes are also separated through steric hindrance known as size exclusion. The size exclusion process controls the rejection of As(III) at pH values 4.5–8.5 because in this pH range, As(III) remains uncharged.[79–81]

The membrane separation mechanisms are based on various mathematical models such as Spiegler–Kedem (SK), Combined-Film-Theory-Spiegler–Kedem (CFSK) *etc.* The latter model is

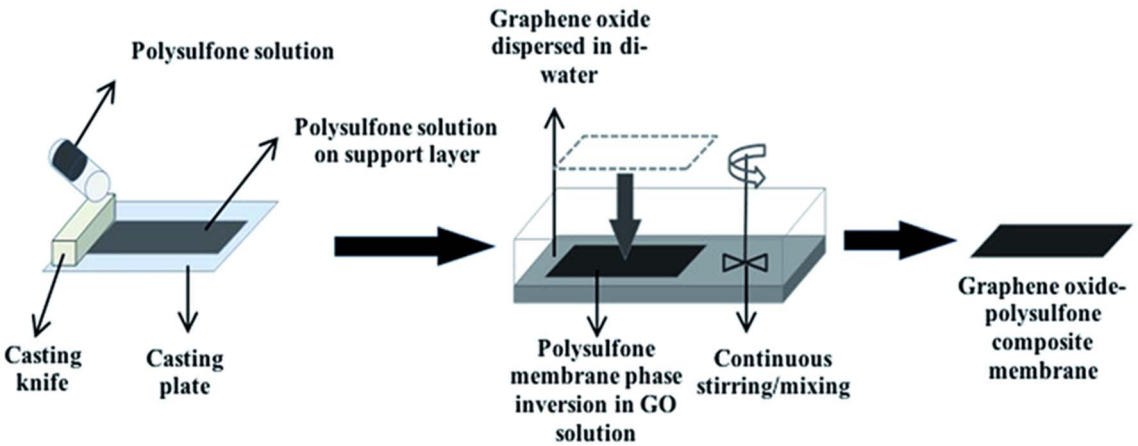

Fig. 2 Phase inversion method for generation of a PSF membrane.[68]

Open Access Article. Published on 07 May 2024. Downloaded on 2/16/2026 7:11:56 AM.
This article is licensed under a Creative Commons Attribution-NonCommercial 3.0 Unported Licence.

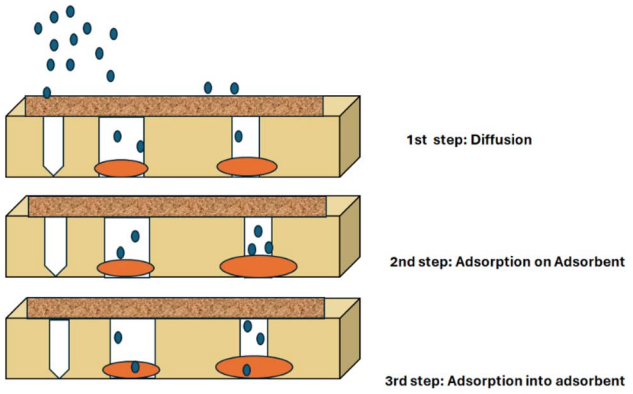

Fig. 3 Mechanism of classical adsorption.

preferred over the former because the former doesn't consider the concentration polarization effect (CPE). The CPE actually causes a decrease in the performance of the system owing to the increased osmotic pressure in the opposite direction at the interface of the feed solution and membrane film.[82] The above-discussed mechanisms ignore the impact of the charges on the surface of membranes; however, the same has been considered in the following mechanisms.

3.3 Donnan exclusion

For compact membranes, Donnan exclusion is a non-sieving mechanism for the rejection of unwanted particles. The mechanism operates on the repulsion produced between the charged membrane surface and ionic species. The steric hindrance also operates at the isoelectric point, where electrostatic repulsions disappear. The pH of solution less than the isoelectric point induces a negatively charged surface of the membrane, which shows greater repulsion towards negatively charged ions, whereas a pH higher than the isoelectric point (IEP) generates a positive charge on the membrane surface, which shows better rejection towards positively charged ions. This reaction occurs due to the ionization of functional groups on the membrane surface, which causes the creation of charges on the external and internal surfaces of membranes.[77,83,84]

3.4 Dielectric exclusion

Yaroshcuk *et al.* reported dielectric exclusion during the separation process by providing an in-depth analysis of this exclusion mechanism. It has been postulated that when an ion interacts with bound electrical charges produced by the ions at the boundary between two materials with different dielectric constants (solvent and membrane matrix), a dielectric exclusion process occurs. According to relative dielectric constants, it is measured that the ion polarizes the two media and forms polarized charge distribution at the discontinuous surface.[84–87]

4. Separation performance of modified PSF membranes

Several two-dimensional materials have been shown to be excellent building blocks for high-performance membranes in recent years. These materials include the graphene family, exfoliated dichalcogenides, zeolites, metal–organic framework (MOF) nanosheets, and dichalcogenides.[88,89] However, graphene oxide–polysulfone based membranes are preferred over other 2D derived materials due to their exceptional strength and stability, resulting in increased durability and a longer lifespan.[90] In addition, GO–PSF based membranes are known for their exceptional permeability and selectivity, which make them ideal for enhancing separation processes. The versatility of graphene oxide–polysulfone membranes is enhanced by their ability to function effectively in a variety of solvents and operating conditions, thereby enhancing their suitability for a broad spectrum of pollutants for water remediation applications.[91–93]

Hydrophilic membranes show minimum fouling by oil droplets as compared to hydrophobic membranes.[94–96] The separation application is affected due to membrane fouling, which results in lowered membrane reusability. Membrane performance in terms of permeability, thermo-mechanical stability and anti-fouling

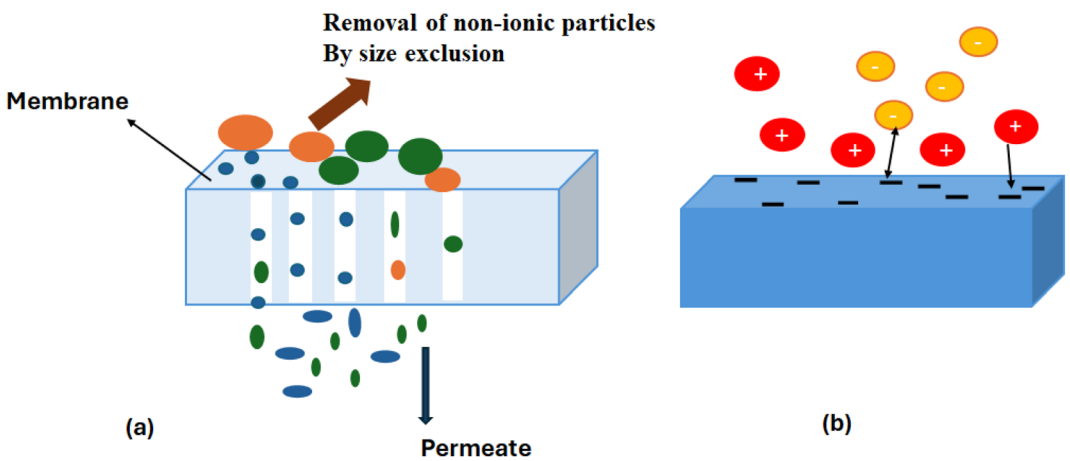

Fig. 4 (a) Removal of non-ionic particles by size exclusion and (b) Donnan exclusion; attraction of positive ions by a negatively charged membrane.

© 2024 The Author(s). Published by the Royal Society of Chemistry

Open Access Article. Published on 07 May 2024. Downloaded on 2/16/2026 7:11:56 AM. This article is licensed under a Creative Commons Attribution-NonCommercial 3.0 Unported Licence.

properties can be increased by adding nanomaterials having an extended surface area with adjustable pore size. Modi *et al.* reported improvement in the efficiency of PSF membranes for oil/water separation through implanting carboxylated multiwalled CNTs/graphene oxide in the hollow region of the membranes. They prepared GO by dispersion of graphite oxide in basic solution and obtained a monomolecular layer of GO. The modified membrane showed high mechanical strength (Young's modulus), anti-biofouling properties and high negative values of zeta potential (high surface negative charge). The reported PSF composite membranes showed high oil/water separation.[55] The separation tendency of hollow fiber membranes (HFMs) can be calculated by measuring antifouling properties, pure water permeability (PWP), permeate water flux through the membrane and efficiency of oil/water separation.[55,97,98]

4.1 Pure water permeability

Pure Water Permeability (PWP) is the flux of pure water without fouling of membranes. The determination of PWP for different samples of hollow fiber membranes (HFMs) has been reported by Modi *et al.* by passing water (for 2 h and at 1 bar pressure) through different samples of HFMs. The PWP can be measured using the following formula (shown in eqn (1)).[99–101]

$$\mathrm{PWP} = Q/n\pi D_i L\Delta P \quad (1)$$

In the above-mentioned equation Q (mL h^{-1}), D_i (m), L (m) and ΔP (Pa) represent the flow rate, inner diameter, fiber length and transmembrane pressure (TMP), respectively.[55]

In a study for oil/water separation, the preparation of oil/water (O/W) emulsion was achieved by blending oil, water and a weighed amount of sodium dodecyl sulphate (SDS) and the resultant mixture was stirred and sonicated for 5 h. As a result, milky white O/W emulsion having a pH of 6.5 was generated.[102,103] The separation processes were applied by feeding O/W emulsion through the HFM sample at one bar for 1 hour. Permeate from HFMs was calculated and dynamic light scattering (DLS) was used to measure the size distribution of oil droplets in permeate. The following eqn (2) was applied to compute the efficiency of each sample (HFMs) to separate O/W.

$$R_{exp} = \left(1 - \frac{C_p}{C_f}\right) \times 100\% \quad (2)$$

In the above equation, C_p and C_f demonstrate the oil-concentration in the permeate and feed, respectively. A UV-visible spectrophotometer was reported to perform calculations regarding oil concentration.[104,105] An increase in the PWP value by using a polysulfone membrane modified with graphene oxide has been reported by Modi *et al.*[55]

Zhao *et al.* reported[106] the determination of permeate water flux from a membrane. In order to determine permeate flux, different samples of membranes were submerged for 24 h in deionized water. Then at operating pressure 1–2 bar, the volume of permeate water within 50 minutes was measured by using the following eqn (3).

$$J_W = Vl(A \times t) \quad (3)$$

where J_W, V, A and t represent the pure water flux (L h^{-1} m^{-2}), permeate water volume, membrane effective surface area and time, respectively. The increase in the pure water flux with rise in the GO content in membranes has been reported by Nasseri *et al.* A GO/PSF membrane with 1.0% GO has been reported to possess the highest flux of water, *i.e.* 512 L h^{-1} m^{-2}.[107]

4.2 Antifouling behavior

The antifouling behavior of membranes is reduction in the deposition of salts, microorganisms, macromolecules and colloids, which cause membrane fouling (Fig. 5). The membrane fouling decreases the membrane life, permeation flux and selectivity.[108,109]

The calculation of the antifouling behavior of different samples of HFMs through measurement of the PWP value after a refusal of oil experiment has been reported. The pure water permeability (PWP) after fouling is called PWP_f. The highest flux recovery ratio (FRR) of 90.5% was reported for CGP-(carboxylated multiwalled GO–PSF)-100 (HFMS), whereas 84.3% FRR was reported for CGP-75 (HFMs). The excellent performance of CGP-100 was attributed to high hydrophilicity and negative surface charge. The hydrophilic membranes containing negative charges allowed the penetration of water molecules and synchronously prevented oil adsorption and hence gave oil free water in permeate.[55] The factors including the measurement of surface charge and electrostatic repulsion are reported for the prediction of the foul-resistance features of the membrane. Moreover, GO reduces the membrane roughness and the resulting smooth surface possesses a better tendency to resist

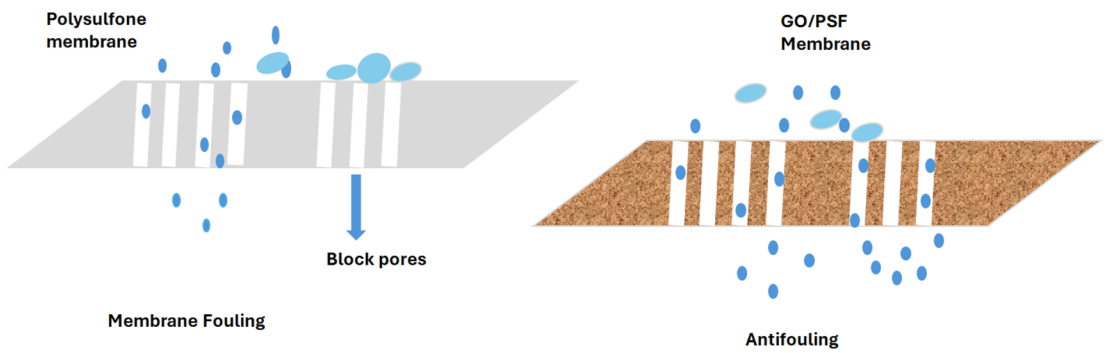

Fig. 5 Fouling and antifouling behaviour of PSF and GO/PSF.

Open Access Article. Published on 07 May 2024. Downloaded on 2/16/2026 7:11:56 AM. This article is licensed under a Creative Commons Attribution-NonCommercial 3.0 Unported Licence.

the membrane-oil adhesion on the surface, which results in the minimum fouling of the membrane. Modi *et al.* concluded that among all the HFM samples, the reduction in the pure water permeability value was found to be lowest in CGP-100 (9.5%). For HFM samples, the flux recovery (FR) increased with the decrease in the CGP percentage. Thus, it can be concluded that polysulfone membranes modified with GO show enhanced separation properties and anti-fouling ability. These graphene oxide polysulfone composite membranes possess significant oil rejection efficiency and are hence used widely for O/W separation.[110]

4.3 Selectivity performance

The term selectivity refers to the selective use of membranes for the separation of certain substances. The changes in the hydrophilicity, contact angle, zeta potential and size of pores are the factors that affect the membrane selectivity performance.[111–113] The membrane having zeta potential and a low contact angle (higher hydrophilicity) shows improved permeability and the membrane having small sized pores decreases the flux or enhances the selectivity of the membrane.[93] Oil rejection experiments have been reported extensively in the literature, which reflect the selectivity of modified GO–PSF membranes for oil/water separation. An oil rejection test was also reported to separate the oil from the emulsion using dead cells by collecting three permeate samples. The measurement of total organic carbon (TOC) of feed and that of permeate was used to evaluate the oil rejection % age. The membrane having 0.1% GO showed maximum oil rejection up to 97.92%. The trade-off between permeability and oil rejection is expected, but this can be adjusted by using the optimum amount of GO. The best agreement between the separation factor and permeability factor is usually achieved through graphical comparison of permeability and selectivity. The reported data showed that membranes which are more permeable to water have less capacity for the separation of oil and water, whereas the membranes with less water permeability have higher potential for the separation of oil from water. The best rejection efficiency was reported for the membrane containing 0.1% GO with low permeability. The membrane having high permeability was modified by minimizing the separation factor.[114] Since the properties of GO alter remarkably upon changing the methods of its synthesis,[115] GO/PSF membranes fabricated from differently synthesized GO show different properties. Salt, oil and various dyes are rejected by using mixed matrix membranes containing GO because of having acidic functional groups, which are the source of negative charge separation on the surface of the membranes.[116] Zeta potential indicates the rejection performance, which measures the charge on the surface of the membranes. The zeta potential of PSF/GO membranes is more negative as compared to PSF membranes, which means that PSF/GO membranes have a more tendency to reject negative ions. The presence of specific functional groups having oxygen which include hydroxyl, carboxyl and carbonyl on the membrane surface is the main reason for the negative values of zeta potential. Initially, rejection increases with an increase in the graphene oxide concentration until the graphene oxide concentration reaches the optimum value and a further increase in the GO content beyond the optimum value causes a decrease in the rejection. The use of GO in optimum amounts causes increases in the flux and oil rejection. This is attributed to the tailoring effect of hydrophilicity and the surface contact angle from the measurement of hydrophilic and hydrophobic properties from interfacial tensions.[117]

5. Characterization of modified membranes

Most of the attributes of membranes depend on the hydrophilic/hydrophobic nature of the membranes, the pore size of the membranes and the rough/smooth appearance of the membranes. The measurement of the contact angle is the best way to determine these characteristics.[118–120]

5.1 Hydrophilic/hydrophobic properties

The use of the water contact angle is reported for the characterization of the hydrophilicity of membranes. The water contact angle decreases with an increase in the addition of isocyanate graphene oxide (iGO) from 0.0 to 0.10%. This water contact angle reduction is a manifestation of increasing hydrophilicity of the membranes. When the iGO amount is increased to 0.15%, then the water contact angle of blended membranes is increased, indicating a decrease in the hydrophilicity of the membrane. The irregular position of iGO in the membrane structure at a concentration of 0.1% iGO causes a reduction in the water contact angle. When the content of isocyanate graphene oxide increases, then the zeta potential decreases on account of the presence of carboxylic groups on the surface layer, which appear on the surface due to hydrolysis upon immersing the membrane in water. The reported experimental results indicate an increase in water flux upon the addition of a small amount of iGO (0.025%) to the PSF membrane. This increase in the flux is due to an increase in hydrophilicity and the formation of straighter and slightly finger like microvoids. But if the iGO concentration exceeds 0.05%, then the water flux decreases. This decrease is due to the agglomeration of iGO, which enhances the viscosity of the membrane and consequently, the membrane porosity is reduced greatly. The decrease in the flux is an indication of the fouling process on the membrane.[121,122]

5.2 Pore size

Brunauer–Emmett–Teller (BET) analysis is used to find out the porosity as well as the surface area of micropores and mesopores in membranes. The BET method determines all the available pores for nitrogen adsorption.[123] Kovtun A. used the BET formula to study the adsorption process for a GO–PSF membrane for organic-contaminant removal from water as shown in eqn (4).

$$Q_e = (Q_m C_{BET} x)/(1-x)(1 + C_{BET} x - x) \quad (4)$$

© 2024 The Author(s). Published by the Royal Society of Chemistry

Open Access Article. Published on 07 May 2024. Downloaded on 2/16/2026 7:11:56 AM.
This article is licensed under a Creative Commons Attribution-NonCommercial 3.0 Unported Licence.

where Q_e represents the number of molecules absorbed at equilibrium, Q_m represents the number of molecules required to cover the whole surface of the adsorbent and C_{BET} is the thermodynamic equilibrium constant.[124] Recently, Lekena N. reported BET results for GO–PSF with a pore surface area of 80.5 $m^2\ g^{-1}$, which increased in the case of the GO–APTES system up to 333.8 $m^2\ g^{-1}$.[125]

5.3 Surface roughness

Van der Waals forces, hydrogen bonding and electrostatic force play a role in the fouling process.[126,127] The flux recovery ratio of composite membranes is greater than that of pure PSF membranes, which reflects the enhanced anti-fouling properties of composite membranes. The increase in hydrophilicity is accountable for the blocking of protein chemisorption on the membrane surfaces.[128] Atomic Force Microscopy (AFM) is used to study surface roughness and fouling. According to AFM, a decrease in surface smoothness enhances fouling.[129] The antifouling properties can be increased by increasing the surface smoothness. The smoothness of the surface is increased after doping iGO (0.05%) and as a result antifouling properties are increased. When the iGO content is increased beyond (0.15%), a valley appears and foulants are absorbed in the valley of the membranes. which results in lowered antifouling properties.[130]

6. Types of modification in GO–PSF membranes

6.1 Modification in GO nanosheets

The synthesis of GO has been reported through the deposition of nanosheets of GO in layers. These sheets were then interconnected through 1,3,5-benzenetricarbonyl trichloride on a PSF support coated with polydopamine (PDA) as shown in Fig. 6.

Liang *et al.* recently reported poly(vinylidene fluoride) modified PSF/GO–Ag nanosheets with dopamine coating. This membrane possessed a water flux of 650.52 L $m^{-2}\ h^{-1}$, a contact angle of 69°, a rejection of 98%, a pore size of 21.16 nm and 81.02% porosity.[132] The separation performance of the mentioned membrane is envisaged by using monovalent salt sodium chloride (NaCl) and divalent Na_2SO_4 salt. The membrane coated with polydopamine showed less than 10% rejection of dyes and almost no rejection of the salt. GO coating on this type of membrane increased the rejection of monovalent along with divalent salts in the range of 6–19% and 26–46%, respectively. The rejection rate varied due to a different number of GO layers deposited on the polydopamine coated PSF support. The rejection of organic dyes was also enhanced by GO coating. The rejection rate for methylene blue was 46–66%, whereas that of rhodamine-WT was 93–95%. The reasons behind the higher rejection rate of R-WT include the higher molecular weight of R-WT than that of MB dyes (size exclusion effect), and the repulsion between the negatively charged surface of the GO (due to the presence of carboxylic groups) coated membrane and anionic R-WT in comparison to MB, which is positively charged. So, the spacing between graphene oxide layers (size exclusion effect) and membrane charges (Donnan exclusion) are the prime factors that determine the rejection performance of GO membranes. The rejection also decreases when the concentration of the solution increases. Na_2SO_4 rejection decreases from 88% to 26% upon an increase in its concentration from 0.1 to 10 mM and a similar effect has been reported for NaCl. The aforementioned observations indicate the great contribution of the charge effect to the membrane separation mechanism. A decrease in the Debye length leads to a decrease in repulsion between the ions and charged membranes, which ultimately leads to a decrease in the rejection rate.[133]

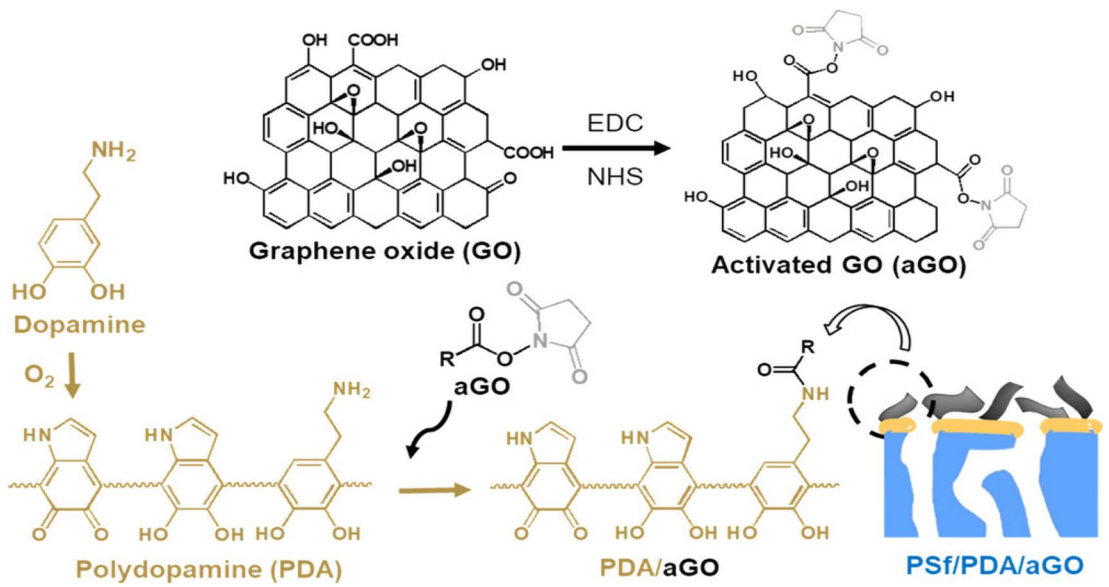

Fig. 6 Modification of a graphene oxide based polydopamine coated polysulfone (GO–PDA–PSF) membrane using 1-ethyl-3-(3-dimethylaminopropyl)carbodiimide (EDC) and *N*-hydroxysuccinimide (NHS).[131]

Open Access Article. Published on 07 May 2024. Downloaded on 2/16/2026 7:11:56 AM. This article is licensed under a Creative Commons Attribution-NonCommercial 3.0 Unported Licence.

6.2 PSF–GO silver nanocomposite membranes

PSF–GO silver nanocomposite membranes are synthesized by blending the solutions of PSF, GO and silver nanoparticles. These membranes have a larger Young's modulus and tensile strength than PSF membranes. The adsorption capacity of silver-decorated graphene oxide (Ag/GO) is often better than that of graphene oxide (GO). This is because GO sheet stacking is decreased and more adsorption sites are provided by the attachment of silver nanoparticles (AgNPs). This decrease in stacking effectively improves the surface area by increasing the gap between the sheets.[134,135] Moreover, the PSF–GO–AG membrane possesses more finger shaped pores and channels with reduced surface-pore size, which results in an enhanced exchange rate in phase separation, increased surface roughness having a mean-surface (R_a) value of 4.40 nm and an increased flux of 66.7 L m^{-2} h^{-1}.[136] Suhalim *et al.* reported a PSF–GO–Ag nanocomposite membrane with a water flux of 141.6 L m^{-2} h^{-1}, a contact angle of 54.71°, rejection of 78.5% and 78% porosity.[137] GO for membrane preparation was obtained from graphite powder (raw material) by employing HM. A GO–Ag nano-hybrid was prepared in a two step process. In the first step, 20 mg GO was mixed with 60 mL PPh_3 (triphenylphosphine), followed by sonication for 1 h at room temperature to disperse GO nanoparticles. 1.4 mg of $AgNO_3$ was separately dispersed in PPh_3. Then both solutions were mixed and sonicated for half an hour. Then the mixture was stirred vigorously, and the temperature was maintained at 80 °C for 24 hours. The GO–Ag nano-hybrid was thus prepared. After that ethanol washing of the nano-hybrid and then drying were performed above room temperature. The GO–Ag nano-hybrid showed higher anti-bactericidal potential due to strong adhesion through PPh_3 between the sheets of GO and AgNPs. A PSF–GO–Ag nanocomposite was synthesized by a solution blending method. First PSF was dried for 24 hours at 80 °C under vacuum and then DMF as a solvent was added to polysulfone resin (PSU) to form a transparent solution. Then this solution was added to the dispersion of GO and silver nanoparticles and then stirred for 6 hours. With the use of an automatic coating machine, the solution was cast into a thin film. Then solvent molecules were evaporated at 25 °C (room temperature) to obtain PS–GO–Ag nanocomposite membranes.

The composite PSF–GO membrane containing silver nanoparticles possesses antibacterial properties against *Staphylococcus aureus* and *Escherichia coli* at a low GO–Ag loading. The antibacterial screening of the membrane was performed using Gram-negative and Gram-positive bacteria. PSU film samples were cut having a width of (50 mm) and then placed into a sterile Petri dish and then bacterial suspension of 0.4 mL was poured onto the film and the sample was covered with a polyethylene square film. Then the antibacterial rate was measured using the following eqn (5).

$$R = N_0 - N/N_0(100) \quad (5)$$

N_0 represents the average number of viable bacteria on neat PSU and N represents the number of viable bacteria on the PSU/GO–Ag film after antibacterial examination. The above-mentioned use is because of their bactericidal capability to prevent bacterial contamination. GO and AgNPs show antibacterial properties (inhibition of bacterial growth) against Gram-positive as well as Gram-negative bacteria. The antibacterial effect of GO–Ag membranes is due to the fact that this material functions as a conducting bridge for the electrons emitted during respiration and fermentation processes to increase the concentration of reactive oxygen species (ROS). The ROS disturbs the balance of the metabolic process of bacteria and also accounts for membrane damage. Besides causing imbalance in the metabolic process and damage to the membranes, this membrane releases Ag ions, which go into bacterial cell walls and have interaction with the biochemical material and cause damage to the nitrogenous base and hereditary material DNA and hence result in decreased cellular activity. Experimental studies indicate that the anti-bactericidal properties are very high for *E. coli* (83%) and *S. aureus* (58.5%) when using the PSU/GO–Ag nano-composite membrane. This difference in antibacterial properties for Gram-positive bacteria and Gram-negative bacteria may be attributed to variations in the nature of the cell membrane and the biochemical composition of each type of bacteria. This type of membrane is therefore considered an excellent candidate for medical uses because of having antibacterial properties.[138]

6.3 PSF/GO zinc oxide membranes

ZnO nanoparticles (ZnO NPs) are beneficial for the membrane process in desalination because of having anti-fouling and antibacterial properties.[139] Compared with other NPs, ZnO NPs are cost effective, biocompatible and considered more appropriate for the preparation of nanocomposites.[140] The ZnO incorporated into the PSF/GO membrane possesses enhanced porosity (83.00 ± 1.18%) compared to neat PSF 52.20 ± 0.28%. These membranes possess a high permeate flux of 35.03 L m^{-2} h^{-1} and a reduced contact angle of 52°, showing more hydrophilic nature than that of PSF/GO.[97] The rejection behaviors of PSF–ZnO–GO (ZG3), PSF polymer and PSF–ZnO (Z2) have been compared by applying humic acid as an organic foulant in solution form. The PSF membrane shows a humic acid rejection of 52% and the ZG3 membrane shows 99% rejection of humic acid. ZG3 showed high permeability and excellent rejection capability. This is because the anti-fouling properties of the membrane are modified due to the hydrophilic character of GO and ZnO–GO NPs. Consequently, the hydrophilic nature decreases the adsorption of organic pollutants within the membranes.[141,142] This increased hydrophilicity is due to the high polarity of ZnO NPs and the presence of epoxy, hydroxyl and carbonyl functional groups on GO nanosheets, which increase antifouling properties or minimize humic acid adsorption on membrane surfaces. These more hydrophilic membranes showed a higher affinity of nanoparticles towards water instead of organic matter, thus causing a minimum hydraulic resistance.[143] The antifoulant behaviour is dependent on the hydrophilicity of the membrane and this hydrophilicity can be changed due to the presence of oxygenated groups in the ZnO–GO nano-hybrid.[144,145] ZnO nano-particles act as an antimicrobial agent in many applications because they are bio-safe

 © 2024 The Author(s). Published by the Royal Society of Chemistry

Open Access Article. Published on 07 May 2024. Downloaded on 2/16/2026 7:11:56 AM. This article is licensed under a Creative Commons Attribution-NonCommercial 3.0 Unported Licence.

materials.[146] ZnO NPs show antibacterial properties against *Bacillus subtilis* and *Escherichia coli* 45, which inhibit bacterial growth and propagation. ZnO NPs disturb the bacterial cell integrity by direct interaction. This also causes the generation of the ROS, which releases superoxide anions and hydrogen peroxide, and hydrophilic membrane surfaces cause less adhesion of *E. coli*. PSF–ZnO–GO shows antibacterial properties due to the increased transfer of electrons to contribute to more ROS generation and hence destroys the bacterial cell.[147,148]

6.4 PSF/GO-bovine serum albumin membranes

Bovine Serum Albumin (BSA) is a protein of serum (derived from a cow) with wide biochemical application[143] and routinely employed as a concentration standard for proteins. BSA can interact with different carbon nanomaterials.[149] Huang *et al.* reported a PSF/GO membrane with a flux of 641.7 L m^{-2} h^{-1} that is 3 times the flux of pristine PSF membranes (229.2 L m^{-2} h^{-1}) under 0.1 MPa pressure. This membrane possessed 98.22% rejection for protein, 47.75 nm pore size, 78.07% porosity and excellent hydrophilic character.[150] Chemically modified BSA has also been used as glue with GO to bind enzymes without any loss in enzyme activity.[151] A dye rejection study is done with the composite (GO–PSF) using intermediate BSA. Its mechanical strength, pore size and contact angle are altered by adding GO to the PSF membrane, which generates a center for binding of BSA. The molecular structure as well as the properties of BSA help it to interact with GO and textile dye (reactive orange), making it possible for the filtration of dye. The pH has a major effect on the dye sorption and filtration mechanism. Experiments have been reported with three PSF membranes different from each other and having different concentrations of GO (2, 4 and 8%) at different pH. It has been proven that addition of 2% GO at pH 7 is the optimal condition for the binding of BSA. The carboxyl group of graphene binds to the amine group of BSA through covalent linkages. Membranes having 2% GO at pH 10 showed maximum dye rejection capability. Besides pH, contact time also affect the filtration mechanism. Higher the contact time between dye and protein molecules, the higher will be the rejection capacity.[141,152]

6.5 PSF/GO matrix membranes

Polysulfone graphene oxide mixed matrix composite membranes (MMMs) have been synthesized by the process of phase inversion.[153] Abdalla *et al.* reported PSF/GO–NH_2 with properties including 68.9% porosity, 65° contact angle, 95.6% oil rejection, 2071 LMH bar^{-1} permeability and maximum hydrophilic character for 0.2 wt% GO–NH_2.[154] Required amounts of graphene oxide (0, 0.05, 0.1, 0.2, and 0.4) and 0.8 wt% relative to PSF are dispersed, which is carried out by sonication in dimethylacetamide (DMAc) for five minutes. A solution of 80% *N*-DMAc/GO, 15% PSF and 5% PVP is prepared by overnight stirring. After this nano-composite solution is degassed in a sonication bath for 10 minutes and then this solution is cast on a glass plate by using a membrane casting machine. Then after half a minute the glass plate is dipped in a deionized water containing coagulation bath for five minutes and then the coagulating film is stored in deionized water (UP, ultra-pure water) for three days.[153]

This composite membrane shows better mechanical and thermal performance as compared to PSF. The reported result is that the tensile modulus and tensile strength are also increased by the incorporation of GO from 153 MPa to 330 MPa and from 3.5 MPa to 5.6 MPa, respectively.[155]

Interfacial polymerization is also a technique used to prepare thin film composite membranes with or without graphene oxide on the top surface of polysulfone membranes. Hosseini *et al.* reported this process including washing (with deionized water), spreading of metaphenylene diamine (MPD) having additives (sodium lauryl sulfate and camphor sulfonic acid) on a polysulfone substrate, initiation of interfacial polymerization by trimesoylchloride solution (in hexane), and removal of excess organic solution, followed by heat treatment of the PSF membrane at 65 °C for the thin film composite membrane. After this washing is done with water and then these membranes are stored in water. For the preparation of a graphene oxide incorporated thin film/layer composite membrane, the same process is followed and the only difference is the use of MPD/GO aqueous solution (Table 1).[156]

7. Applications of GO–PSF membranes

7.1 Removal of organic pollutants

Bisphenol A (BPA) is generally used for the synthesis of plastics and found as a pollutant in small amounts in water due to its low solubility. BPA is a hazardous pollutant of water bodies.[107]

Table 1 Comparison of the properties of various types of modified GO–PSF membranes

Types of membranes	Pore size (nm)	Porosity (%)	Rejection	Contact angle	Permeate flux L m^{-2} h^{-1}	Operating conditions	Pollutants	Ref.
GO–PDA–PSF nanosheets	21.16	81.02	98%	69°	650.52	37 °C, 0.1 MPa	BSA	131
PSF/GO–Ag nanocomposite membrane	2.1–2.4	78%	78.5%	54.71°	141.6	37 °C, 7 bar, stirring at 300 rpm	Fe^{2+}	132
PSF/GO–ZnO membranes	41.40	83	99%	52°	35.03	5 bar sheet thickness 4 cm	Organic pollutant	97
PSF/GO BSA membranes	47.75	78.07	98.22%	57°	641.7	0.1 MPa	BSA	150
PSF/GO matrix membranes	2.44	68.5	95.6%	65°	207.1	1–7 bar	Oil	154

Open Access Article. Published on 07 May 2024. Downloaded on 2/16/2026 7:11:56 AM. This article is licensed under a Creative Commons Attribution-NonCommercial 3.0 Unported Licence.

This pollutant disturbs the endocrine function. It can cause liver damage, (THD) and cancer.[157] Traditional methods are not good for the removal of BPA. For the removal of this pollutant, membrane physiochemical separation techniques are feasible.[158]

Nano-composite membranes show better performance when regarding BPA removal and permeate flux. This permeated flux has linear relationships with the GO content of the membranes, meaning that permeated flux increases when the graphene oxide content increases. The BPA rejection efficiency is highest for the nanocomposite-membrane having 0.4% GO. There are various factors that affect the BPA removal efficiency. The BPA rejection efficiency is enhanced by lowering the operating pressure and enhancing the BPA concentration. When the BPA concentration is high, then less time is required for the removal of BPA because of enhanced electrostatic repulsion of negative charge with the membrane negative charges. pH also affects the rejection efficiency of BPA. Increased pH results in increased electrostatic repulsion and hence leads to higher BPA rejection and also reduced operating time.[107]

Methylene Blue (MB) is a cationic dye and hazardous because its exposure results in jaundice and an increased heart rate. Hence, removal of dye from water is essential to avoid its health risks.[159] PSF exhibits low adsorption of dye. An increase in the adsorption of MB dye has been reported upon using a PSF/GO nanocomposite (generated by a phase inversion method). The adsorption efficiency increased approximately 20% for PSF/GO composite membranes in comparison to PSF membranes. This increase is attributed to the negatively charged groups of GO on the polysulfone membrane surface. The observed ease in the absorption of methylene blue was due to electrostatic interactions between positively charged MB and the negatively charged membrane surface.[90]

PSF modified with GO (1% weight) exhibits organic removal up to 70%. The doping of GO in PSF gives additional properties to the membranes.[160] Ion adsorption and Gibbs Donnan exclusion are operative mechanisms in the rejection performance of membranes. GO imparts negative charges to the membrane on account of deprotonated carboxyl groups. The negatively charged surface repels anionic species and facilitates the adsorption of positively charged metal cations. Higher the quantity of GO in the membrane, easier will be the adsorption of dissolved ions (having position charge) and hence lower the total dissolved salt concentration (TDS) in water.[161] Ammonia exists in the form of ammonium ions in water bearing positive charge. The pH of natural rubber wastewater was 6.6. This phenomenon shows that equilibrium shifts towards the ionized form (ammonium ions) having a positive zeta potential effect on the separation properties of membranes particularly for charges to be separated. These positively charged ions are adsorbed on the negatively charged membrane surface (Table 2).[162]

Table 2 GO–PSF derived materials for the removal of organics[a]

Adsorbent	Adsorbate	Adsorption capacity (mg g^{-1})	Parameters	Ref.
Alg/GO	Methylene blue	12.64	25 °C, pH = 7.78	163
GO–PAMAM	Oil	120	4 recycles	164
PSF–TiO_2/GO	TDS (from rubber)	NA	pH = 8–8.5, C 335 mg L^{-1}	160
(P(Aam-IA)/GO–PEI)	Azo dyes (cationic (crystal violet))	390.6–774.46	0.2% GO wt	165
SA/GO@Fe_3O_4/CS	Methylene blue	21.325	5 recycles	166
	Neutral red	44.654		
	Safranine T	44.313		
CS/AAm/IA/GO	Methylene blue	247.47	C_0 5 mg L^{-1}, pH = 8	167
rGO/MMT/XDV	Rhodamine	482	5 adsorption/desorption cycle	168
rGO/XDV	Toluene	500		
β-CD/GO	Organic dyes (methylene blue)	76.4	70 °C, 60 min, adsorbent C = 0.04 g L^{-1}	169
SA–GO	Tartrazine	420.36	Aqueous medium	170
MOF-525/GO	Tetracycline	436	303 K, pH = 3	171
SA–HEC/GO	Crystal violet	312.72	pH = 5	172
GO	Methylene blue	33 333	25 °C	173
rGO	Methylene blue	2000		
Fe_3O_4@GO@AHSA	Methylene blue	286	37 °C	174
PSF/GO/poly(MMA-*co*-GMA)	Oil	NA	C 50–1000 mg L^{-1}	104
	BSA			
PSF–MMMs–GO	Oil	NA	C 0.05–0.8 wt%	114
GO–CuO@CA–PES	Methylene blue	37.1	273 K, $C = 1 \times 10^{-5}$ M & pH 9	175
	Rhodamine blue	30.05		
	Congo red	20.20		
	Methyl orange	6.79		
RGO–PEG–ZnO	2,4-Dichlorophenol (2,4-DCP)	570.641	25 °C, pH = 7	176
	Phenol	531.804		
	2-CP	511.248		
	Bisphenol-A (BPA)	485.756		

[a] NA: data not available.

© 2024 The Author(s). Published by the Royal Society of Chemistry

Open Access Article. Published on 07 May 2024. Downloaded on 2/16/2026 7:11:56 AM. This article is licensed under a Creative Commons Attribution-NonCommercial 3.0 Unported Licence.

7.2 Removal of salts

Desalination is an important method for fresh water augmentation by removal of salts and minerals from saline water.[177] Membranes used for the desalination process require modification in terms of antifouling properties, water flux and salt rejection. The development of nano-fields leads to addition of nanomaterials in polymeric membranes for desalination techniques. Advanced membrane materials have an influence on desalination processes, including reverse-osmosis, membrane distillation, forward-osmosis, pervaporation, and electrodialysis.[178]

Desalination membranes require hydrophilicity. For increasing hydrophilicity and salt rejection, PSF membranes are modified with GO. MGO has amphiphilic nature, and water molecules are adsorbed first at terminal hydroxide (hydrophilic nature) and then rapidly diffused in the carbon core (hydrophobic and hence a creating water channel), which enhances the permeation flux. This thin carbon sheet when incorporated in PSF increases the properties of PSF at low concentration. Besides increasing the salt rejection, water uptake also increases the water uptake with increase in GO in the membranes. This relationship is due to the presence of hydrophilic sites in GO, which result in increase in the uptake of the solvent. Three factors affect the water uptake potential of the membranes and are the membrane morphology, number of hydrophilic sites in the membranes and pH. GO doping also increases macro-voids in the PSF sub-layer. This increase in macro-voids results in increase of the uptake capacity of the membranes. Solvent uptake increases with increase in pH in GO/PSF membranes. Through ion dipole forces, negative charges (on GO) interact with molecules of water, resulting in more water uptake. When pH increases, hydrogen ion concentration decreases and hence equilibrium reactions shift toward the right, producing more negative ions.[179]

For salt rejection PSF/GO nano-composite membranes can also be used. A salt rejection study has been performed through finding rejection in 1000 ppm Na_2SO_4 and NaCl solution at various operating pressures. The solute rejection is directly proportional to GO content in composite membranes. Membranes having 2000 ppm GO content show an optimum rejection of 72% for Na_2SO_4 at an operating pressure of 4 bar. The low pH of feed solution induces low rejection. This low rejection is because of small dissociation of ionizable species and reaction shift toward the left, which produces less negative charge or fewer cation exchange groups. This also indicates that the membrane has negative charge on the surface. The functional group dissociation is also a cause of the appearance of negative charges found on graphene oxide. At higher applied pressure, the rejection efficiency of PSF/GO is decreased as compared to that at low pressure. The pristine PSF membrane shows poor rejection efficiency as compared to PSF/GO nano-composite membranes. The rejection efficiency is highest when 2000 ppm GO is doped into PSF membranes. PSF/GO membranes show higher rejection of Na_2SO_4 as compared to NaCl. This increased rejection of Na_2SO_4 is because of negative charges on the membranes, which strongly repel SO_4^{2-} in contrast to chloride ions due to smaller hydrated ionic size.[180] Hence, the low rejection of NaCl by the membranes is attributed to the small effect of Donnan and size exclusion. GO nanosheets are incorporated in polysulfone to get a polysulfone graphene oxide composite membrane support layer. After this polyamide layers are generated on polysulfone GO through interfacial polymerization for a thin film composite for forward osmosis (TFC-FO membranes). The membrane permeability for water molecules is increased by a suitable amount of GO in PSF.[112] The problem of water storage arises due to economic development and population growth. To overcome this water shortage, one solution is sea water desalination for substituted resources of water. The technology of forward osmosis (FO) membranes is implemented for desalination[181] and wastewater treatment.[182,183] The FO membrane is semi-permeable and across it a gradient of osmotic pressure induces the transport of water. TFC membranes show high permeability for water molecules and low reverse permeability for solute molecules. The FO membrane containing a thin film composite has a slim active layer, which is formed from polyamide with a permeable structure. This polyamide layer (PA) is liable for large salt rejection and promotes the transport of water molecules. GO is an excellent material to modify TFC-FO membranes because of possessing various oxygen containing functional groups.[184] GO with a high surface area to volume ratio facilitates effective interaction with the matrix of polymer. The addition of GO also reduces the contact angle that corresponds to higher hydrophilicity and this increased hydrophilicity results in increased water permeability for composite membranes. The addition of GO beyond 1% causes the reduction of favorable structural properties, which affects layer preparation for PA rejection and water permeability. This reduction in permeability and rejection for higher contents of GO is because of unequal GO dispersion in the PSF and leads to membrane formation having smaller pore size, resulting in an adverse effect on membrane salt rejection.[185,186]

7.2.1 Regression error. Regression models are applied to study the statistical effects of various parameters on the desalination performance of membranes. The given relationship determines how the empirical equation is employed to approximate the experimental data regarding the independent process variables.

$$Y = b_0 + \sum_{i=1}^{n} b_i\ X_i + \sum_{i=1}^{n} b_{ii} X_i^2 + \sum_{i=1}^{n-1} \sum_{j=i+1}^{n} b_{ij} X_i X_j$$

where X_i and X_j are the dimensionless coded variables, Y is the expected response, b_0 indicates the constant, b_i, b_{ii}, and b_{ij} are the linear, quadratic, and interaction regression coefficients, and n is the number of design variables.[187] A determination coefficient (R^2) is also used to elucidate the model data derived from experimental data and it also determines the removal efficiency of the membrane. The ratio of the model's sum square to the sum square of y was defined as R^2.[188]

$$R^2 = \frac{SS_{mod}}{SS_{tot}}$$

7.3 Removal of metal ions

The biochemical process within the human body involves some heavy metals like Zn, Cu and Mn. Unfortunately, excessive exposure to these metals causes an adverse effect and some

Open Access Article. Published on 07 May 2024. Downloaded on 2/16/2026 7:11:56 AM. This article is licensed under a Creative Commons Attribution-NonCommercial 3.0 Unported Licence.

heavy metals including cadmium, mercury and lead are toxic because these metals are non-biodegradable and hence can store in the human body. These metals should therefore be removed from water.[189]

Commercial GO based nano-filtration membranes are available for heavy metal rejection. These commercial membranes have been used successfully for the treatment of copper, cadmium, manganese, and lead under a pressure of 4 bar for 1000 mg L^{-1} initial concentration of heavy metal. Metal salts are successfully rejected according to Donnan exclusion theory. There is a significant role of Donnan repulsion as well as the adsorption mechanism in rejection. This composite membrane shows greater adsorption (Table 3) due to the existence of reactive functional groups, including the carboxylic group on the membrane's surface and due to porous additives in the membrane's structure.[77] Arsenate rejection up to 83% occurs at basic pH. The predominant mechanism in arsenate rejection is Donnan repulsion.[190] Lead is a heavy metal and exists in divalent form. Lead damages the kidney, brain and reproductive system in humans. Uncoupling of ionic species through nano-filtration membranes is dependent on membrane charges and the membrane pore radius. A porous membrane possessing smaller pores has potential for the retention of charged species, and highly charged membranes have more potential for the exclusion of co-ions (similarly charged ions to membranes). A lead rejection experiment has been reported at various pressures 1, 2, and 3 bar at solution pH 6. After 30 minutes, the permeate sample is collected and quantitative analysis is performed by measuring rejection for lead ions. At 1 bar pressure, 1% GO content membranes are reported to show high rejection. PSF/GO nano-composite membranes exhibit lower flux for lead nitrate solution as compared to pure water. The flux decreased but it was still higher than the flux when only PSF membranes were used. When only the PSF membrane was used, the flux for lead nitrate was higher than the pure water flux. This increase is due to pore opening and the absence of graphene oxide that can retain the lead ions. Membrane rejection efficiency decreased with increase in pressure. A higher pressure results in increased permeability for water molecules, which causes lead ions to pass through membranous pores by convection. GO addition develops negative charges on the membrane, which cause the adsorption of lead ions (positively charged).[191]

Donnan exclusion (charge–charge repulsion) in arsenic removal occurs from water when using nano-filtration membranes having negative charges. As (5) and As (3) have different rejection capacities by the membranes when the concentration of arsenic feed water solution is changed. By enhancing the concentration of arsenic feed, the rejection efficiency of As(v) is also expanded from 60% to 90% by increasing the concentration of arsenic feed from 10 to 316 μg L^{-1}. The rejection efficiency of As(iii) is decreased by increasing the arsenate feed water concentration. The arsenate rejection efficiency is decreased to 5% from 28% by increasing the arsenic feed concentration from 10 to 316 mg L^{-1}. The rejection efficiency of As(v) decreases by decreasing the pH. However, the As(iii) rejection efficiency is affected by the pH. This information is obtained on the basis of membrane pore size and charge. Donnan exclusion mechanisms are the reason for high rejection efficiency instead of relatively large membrane pore size. The separation results show that for highly charged species As(v) rejection the employed mechanism is Donnan exclusion. The reported arsenic rejection survey determines that the main factors affecting the separation (As(v) and As(iii)) are the pH and concentration of bulk solution. The separation of As(v) was found to be within 60–90% for the feed concentration of arsenic of 10 and 315 mg L^{-1}. The rejection was decreased to 5% by adding 10 mM NaCl. There, rejection is due to electrostatic

Table 3 GO–PSF derived materials for the removal of inorganics[a]

Adsorbent	Adsorbate	Adsorption capacity (mg g^{-1})	Parameters	Ref.
GO–Ch	Cu cation	58.5	20 ± 2 °C, pH = 7, 20 g L^{-1}	196
GO–Fe_3O_4/PSf	NaCl	NA	27.79 g mL^{-1}	197
rGO@CDs	As(v)	87.6	100 μg L^{-1}, 40 bar	198
PSF–GO/Pt	Nitrate	NA	50 mg L^{-1}, 3 bar	199
PSF–PVA–SA–GO	As(iii)	NA	5 mg L^{-1}	200
PSF–MMt–GO	Hg(ii)	144.89	150 mg L^{-1}, pH = 2	201
PSF–ZnO	Cu(ii)	84	pH = 7	202
GO–Fe_3O_4	Cu(ii)	18.1	Basic conditions	203
Sr–GO–MMT–PSF	Cu(iii)	101.83	pH = 6	204
GO–EDA–Al_2O_3	Na^+, Mg^{2+}, SO_4^{2-}	NA	pH = 7–11	205
Lignin–PNMA–rGO	Pb(ii)	753.5	pH = 5.1	206
GO–EDTA–CS	Hg(ii)	324	pH = 5.10–8.30	207
	Cu(ii)	130		
GO/PEI	Cu(ii)	150.9	pH = 5.5	208
MXene/GO	U(vi)	1003.5	pH = 6.0, 298 K	209
CS–GO–DO/ZnO	Uranium	561.09	—	210
Lignin/GO–PSF	Pb(ii)	71.32	pH = 7.0, 300 rpm	211

[a] NA: data not available.

© 2024 The Author(s). Published by the Royal Society of Chemistry

Open Access Article. Published on 07 May 2024. Downloaded on 2/16/2026 7:11:56 AM. This article is licensed under a Creative Commons Attribution-NonCommercial 3.0 Unported Licence.

repulsion that exists between the co-ion $HAsO_4^{2-}$ and the negatively charged membranes. The decrease of rejection efficiency by adding salt is because of charge exclusion decrease due to increasing salt concentration in the test solution, therefore lowering the separation of As(v) oxyanions. According to Hodgson, the ionic separation of different species can be enhanced using solutions of various solutes due to the presence of more permeable ions of the same charges.[192] Hence the rejection of As(v) can be increased by the addition of bicarbonate ions that are more permeable than As(v). When feed arsenate concentration increases, As(iii) separation decreases. This decrease is because when feed arsenate As(v) and As(iii) concentrations increase, the diffusion and convection of uncharged species increase. This increase in the diffusion and convection of As(iii) results in a decrease in its rejection. At low pH, As(v) rejection is also low and rejection of As(iii) is independent of the pH. There are multiple factors that contribute to the decrease in the rejection of As(v) at low pH. In other words, the negative charges on the membranes are less at low pH, thus decreasing the Donnan exclusion for oxyanions of As(v). The As(iii) rejection is independent of pH in the range of 4.5 to 8.5. This is because it remains unchanged in this range. The As(iii) removal is due to steric exclusion, which is small and therefore its rejection is not affected by the change in the membrane properties.[193]

Dhara *et al.* reported a lignin/GO–PSF membrane (synthesized by phase inversion) for the removal of Pb(ii) from water. Filtration operations were performed using an aqueous solution of Pb and Eosin Y dye. The electrostatic interaction between Pb^{2+} ions and negatively charged Eosin Y molecules created a bigger Eosin–Pb complex. According to the best-model-fit, the adsorption process may entail multilayer physisorption.[194]

The separation performance of a ZnO–Al_2O_3–PSF mixed matrix membrane has been checked in terms of permeation fluctuation and removal of ions (heavy metal), including As(v) and Pb(ii). The improved hydrophilicity, surface charge, and porosity of the synthesized membranes allowed the removal of As and Pb with efficiencies of 87% and 98%, respectively. Filtration experiments have been reported at different pressures. Increasing the number of nanoparticles (Zn and Al_2O_3) gradually increases the rejection of heavy metals and permeation flux; however increasing the number of nanoparticles beyond an optimum number results in decrease in the rejection efficiency of the membranes and this is because excess nanoparticles lead to larger porosity. Steric and Donnan exclusion is the operating mechanism for the rejection of ions. As(v) is an oxyanion and it exists in the hydrogen arsenate form ($HAsO_4^{2-}$) and dihydrogen arsenate (H_2AsO_4) near neutral pH and removal of As(v) is in the combined form. As negative charge causes electrostatic repulsion by anionic species on the membrane surface and Pb^{2+} cations cause electrostatic attraction with the negatively charged membrane surface. Dielectric exclusion also contributes significantly to ion rejection, and it also explains the high rejection that is observed in the nanofiltration membrane in ionic solution having divalent counter ions. As(v) exists in the monovalent state $H_2AsO_4^-$ and hence it is affected slightly compared to Pb^{2+}.[195]

7.4 Removal of radionuclides

Graphene oxide has high potential for radionuclide sorption. GO synthesized by Hummers' method (HGO) exhibits a high sorption capacity of radionuclides as compared to GO generated by the Brodie method (BGO). BGO shows fewer defects and contains a high relative concentration of hydroxyl groups and even functional group distribution over the surface.[212] Fig. 7 presents an illustration of the formation of HGO defects and sorption sites. HGO exhibits a larger number of carboxyl and carbonyl groups possessing numerous holes and increased sorption capacity of HGO towards radionuclides due to interactions with the carboxylic group on GO flakes.[213] HGO is used to produce reduced graphene oxide (rGO), which is then oxidized by HM, resulting in the formation of defective graphene oxide (dGO). This dGO exhibits enhanced sorption of radionuclides due to a larger number of defects and doubly bonded oxygen. This rGO is generated by thermal standard HGO molting.[214] This reduced graphene oxide undergoes further oxidation, which results in the multiplication of defects. The gas pressure inside the interlayer is developed due to the high rate of generation of carbon oxides and explosion.[215] The strong explosion and heating result in the maximum surface area and maximum number of defects.[216–218] The carboxylic group which is present inside the hole of dGO is the sorption site for the elimination of radioactive waste from aqueous solution.

The sorption of U(vi), Am(iii), and Eu(iii) has been reported for the examination of graphene oxide defects and the HGO standard. U(vi) is present in the form of a cation that is the

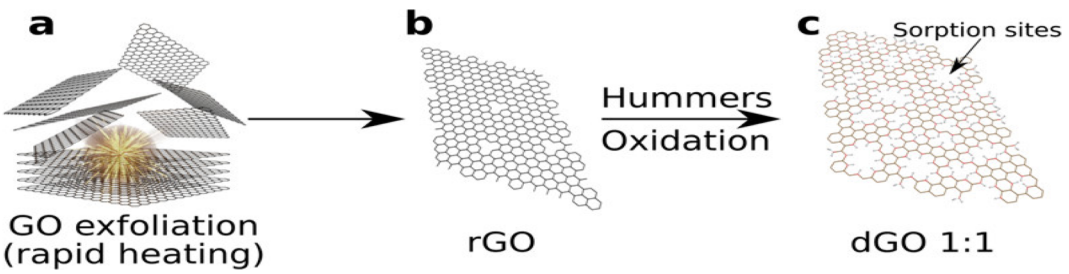

Fig. 7 Scheme for the preparation of defective GO: (a) explosive thermal-exfoliation of GO, (b) Hummer's oxidation of defective rGO and (c) dGO with sorption sites.[219]

Open Access Article. Published on 07 May 2024. Downloaded on 2/16/2026 7:11:56 AM. This article is licensed under a Creative Commons Attribution-NonCommercial 3.0 Unported Licence.

uranyl cation UO_2^{2+} possessing +2 total charge and +3.2 effective charge. Am(III) has +3 charge. dGO has great sorption potential for both U and Am over a wide range of pH. dGO shows higher sorption because of higher carboxyl group concentration than HGO. Hence the sorption isotherm for radionuclides has been applied to find functional group contents. The sorption capacity of dGO is 15 times more for U(VI) and 2 times for Am(III) as compared to pristine HGO. Radionuclides bind to various GO types, and carboxylic acid present on the boundaries of small holes is the reason for the sorption of cations including uranyl cations. dGO exhibits 15 times more sorption for U(VI) and 2 times for Am(III). This huge increase in the sorption of uranyl is due to even uranyl distribution over the dGO flakes. This uranyl cation is bound to the carboxylic group. This carboxyl group is found inside of small holes in dGO. dGO shows higher sorption capacity due to this increase in the defect and hence can be used in the treatment of radioactive waste.[214]

Graphene is considered an excellent adsorbent because of its high surface to volume ratio.[220] But graphene has one disadvantage; it causes aggregation and hence promotes the precipitation of aqueous solution that hinders its application. The dispersion properties can be increased by graphene oxide for which graphene is the precursor, and it can be applied as an adsorbent for radionuclides. Adsorption is a surface phenomenon and is regulated by surface functionalities. Graphene is modified with functional groups to enhance the adsorption potential for pollutants by increasing dispersion in solution and decreasing the self-aggregation.[221] Amidoxime is grafted on graphene oxide. Amidoxime has hydroxyl and amino groups that are used for improving the performance of adsorbent adsorption for aqueous solution containing heavy metal ions.[222] pH also affects the adsorption of radionuclides on poly amidoxime reduced graphene oxide (PAO–rGO). The adsorption of Sr(II) on the PAO–rGO composite increased from 7–73% in the pH range 2–11. The pH change can increase or decrease the metal ion adsorption by changing Sr(II) distribution in the solution and charges on the adsorbent surface through dissociation of the functional group.[223] When pH is low, the functional group on the adsorbent surface is less dissociated. As a result, less Sr(II) is adsorbed and increasing pH causes negative charges on the adsorbent surface and increases the adsorption potential.[224] The zeta potential at different pH is examined to study the pH effect on radionuclide removal. The membrane or adsorbent surface is positively charged at pH less than 4.2 due to protonation of the PAO group. However, when pH is more than 4.2 the composite membrane gains a negative charge, which causes an increase in the binding of positive radionuclide ions. Hence, the trivalent ions having a positive charge on Eu possess a higher binding than positively charged divalent ions Co. From the above-mentioned information, it can be concluded that the adsorption of radionuclides is due to the interaction of ions having opposite charges.[223] Sr is a radionuclide, and it enters the body and replaces calcium and it damages the organs of the body and is hence responsible for causing diseases.[225] Hence it is very important to remove strontium from wastewater. The interlamellar spacing of GO using polyvinyl alcohol increases, which enhances the exposure of the active site and increases the adsorption capacity of GO towards strontium. The PVA/GO aerogel possesses monolithic morphology. This unique morphological feature endows the aerogel with a unique feature of convenient separation. The reported result indicates that the adsorption of strontium does not depend on temperature. PVA/GO at pH 7 exhibits a high removal efficiency of up to 79.13. Under a low pH or acidic environment, the carboxyl group of GO is protonated and the Sr(II) adsorption is decreased because of electrostatic repulsion.[226] Under a higher pH or basic environment, the deprotonation of the carboxyl group of GO occurs, and the presence of the hydroxyl group therefore destroys the H bond and as a result, aggregation of GO leading to reduced active sites has been observed. The selectivity of PVA/GO can be checked in the presence of various competitors like Na^{1+}, K^{1+}, Ca^{2+}, and Mg^{2+}. The competitive effect depends on the nature of Sr(II) ions, and this ability follows the decreasing trend $Mg^{2+} > K^{1+} > Na^{1+}$. This competitive ion decreases the adsorption performance of Sr when the ratio is set as 40/1. Moreover, the hydrated ionic radius of divalent ions is comparable to that of strontium, and thus they also have a much greater inhibition effect on the immobilization of Sr^{2+}. The adsorption mechanism of Sr includes two aspects: interaction developed between the pi electron domain of GO sheets and Sr(II) and strong complexation between Sr(II) and COOH/OH groups. Both of the above aspects decrease the interlamellar spacing among GO layers and hence cause deformation along GO planes.[225]

8. Simulation studies of PSF membranes

Simulation studies give information related to the microstructure of nanocomposite polymer membranes. In addition, these studies give fast and computationally inexpensive information about calculated properties, which include end to end distance, d spacing of microstructural plates and free volume of the polymer chain with high accuracy compared to experimental data.[227]

Force gives a statistically consistent set of system configurations along with a complete description of quantum mechanics.[228,229] Within a statistical framework, discrete and random samples are used in the Monte Carlo (MC) simulation approach. It is frequently used in thermodynamic systems, especially when examining atomic migration and related phenomena. Defects in layered 2D nanomaterial membranes were studied using Monte Carlo simulations in order to understand how their layered structure forms and how this affects molecular transport, namely permeability and selectivity.[230,231] Independent pathways have different probabilities of permeability because molecules prefer paths with a lower barrier. The effective path length was given by eqn (6)

$$L_e = \frac{n_T}{\sum_{i=0}^{n_p} (\alpha L_V + L_H)^{-1}} = \frac{1}{\zeta}\left[\frac{n_p}{\sum_{i=0}^{n_p} (\alpha L_V + L_H)^{-1}}\right] \quad (6)$$

© 2024 The Author(s). Published by the Royal Society of Chemistry

Open Access Article. Published on 07 May 2024. Downloaded on 2/16/2026 7:11:56 AM.
This article is licensed under a Creative Commons Attribution-NonCommercial 3.0 Unported Licence.

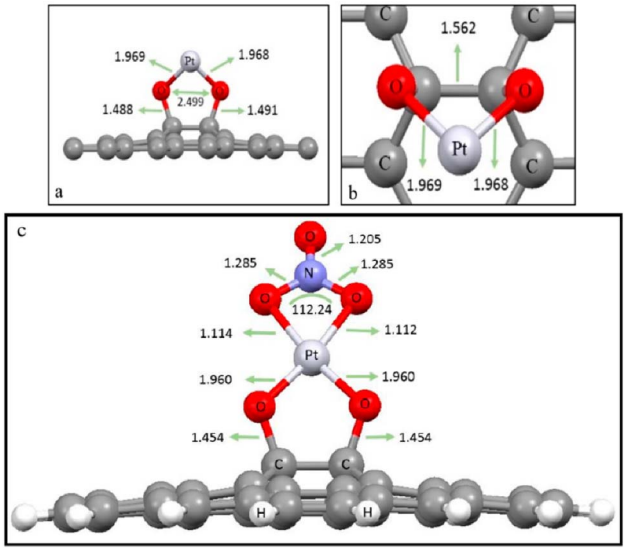

Fig. 8 (a and b) Side view and top view of the optimized position of Pt-nanoparticles on the surface of GO, and (c) optimized nitrate-interaction with the GO/Pt surface and bond lengths (Å).[199]

where n_T and n_P are the total number of probes and the number of probes passing through the membrane; ζ is the ratio of n_T and n_P, α is the weighting factor, and L_V and L_H are the vertical and horizontal path length, respectively. Since the path length that water molecules take through the laminate determines the water permeability, which is inversely proportional, the average permeability P is therefore determined using the harmonic mean as the function that is followed.

$$< P \geq \frac{1}{r_H L_e}$$

where r_H represents the horizontal-resistance per unit-length. The salt-rejection was given as eqn (7)[232]

$$R = 1 - \frac{C_p}{C_m} = \frac{\frac{A}{B}(\Delta p - \Delta \Pi)}{1 - \frac{A}{B}(\Delta p - \Delta \Pi)} = \frac{\frac{P_w V_w}{P_s R_g T}(\Delta p - \Delta \Pi)}{1 + \frac{P_w V_w}{P_s R_g T}(\Delta p - \Delta \Pi)} \quad (7)$$

The atomic-scale investigation of mass transport theory in graphene-based membranes is greatly aided by molecular mechanics-based MD simulation.[233,234]

Recently, Khajouei *et al.* performed the simulation investigation (Fig. 8) of a GO–Pt/PSF membrane for nitrate removal using simulating software OPEN-MX. The results showed that 0.75 wt% GO/Pt nanoparticles have the highest stability in the membrane.

Yang *et al.* reported a simulation examination of a single layer nanoporous GO membrane (NPG) for the desalination and removal of small organic pollutant molecules from water. Seven organic molecules including methanol, phenol, 2-propanol, pyrrole, *n*-nitrosodimethylamine and urea were considered to recognize the molecular factors that promote organic removal. The reported results demonstrated that water-organic permselectivity for small pores having hydroxyl functionalities is higher. The pore-size sieving mechanism was observed for the separation of organic molecules. Fig. 9 shows that transport through the NPG membrane decreases with an increase in molecular size.[229,235]

9. Challenges and future prospects

The performance of PSF–GO derived membranes in removing pollutants from contaminated water has been impressive. However, there are several challenges associated with scaling up their applications. Firstly, research has demonstrated that the issue of GO aggregation within polymeric networks can be addressed through the functionalization of graphene oxide.

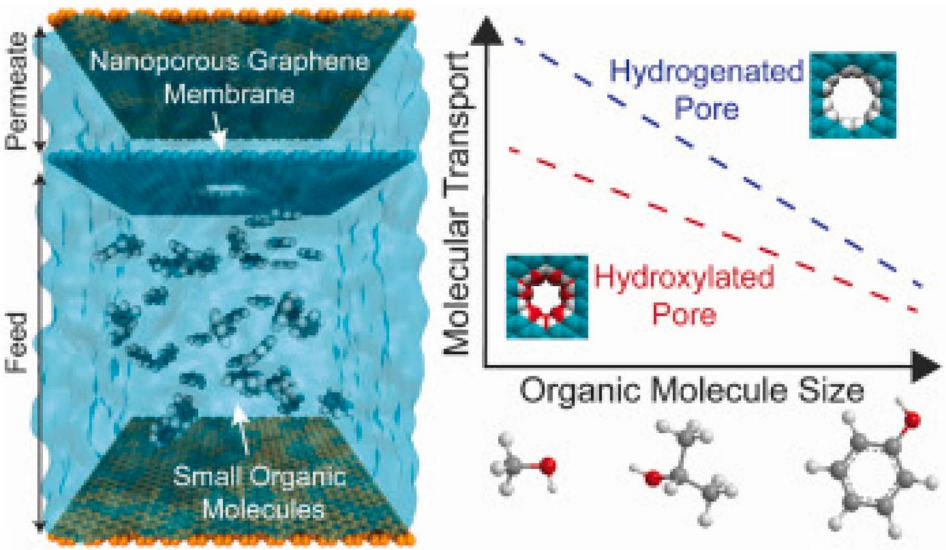

Fig. 9 Illustration of the performance of the NPG membrane for the removal of organic molecules.[229]

Open Access Article. Published on 07 May 2024. Downloaded on 2/16/2026 7:11:56 AM. This article is licensed under a Creative Commons Attribution-NonCommercial 3.0 Unported Licence.

This functionalization prevents agglomeration in polymer systems, particularly in the presence of sulfuric acid. Furthermore, sulfonated graphene oxide can be readily produced from graphene oxide and features negatively charged clusters that enhance hydrophilicity and dispersion and prevent fouling.[236] Secondly, limited adhesion between the GO layer and the substrate, since GO films are commonly produced using the drop-casting method, poses a challenge for the composite structure. Nevertheless, studies have demonstrated that the weak attachment can be improved by applying surface modification techniques.[237]

In recent times, a new nano-architecture has been introduced that utilizes GO-assembled 2D channels with a specific interlayer height of a few nanometers. This design is intended to facilitate rapid transport and enable specific gas sieving through the use of carefully crafted external forces.[238] In order to enhance the hydrophilicity of a film, various techniques have been employed, including surface coating, interfacial polymerization, and layer-by-layer assembly, each presenting specific challenges. While surface coating effectively reduces the number of surface pores on the membrane, it does not affect the membrane's internal pores. However, the intricate procedures involved in polymerization techniques, including interfacial polymerization, increase the yield of the film. An alternative approach is to improve the antifouling performance by increasing the hydrophilicity of the film by incorporating hydrophilic nanofillers into the bulk polymer network to produce a hybrid ultrafiltration membrane.[239]

The majority of existing research has focused on the individual performance of each pollutant. However, it is extremely difficult to adsorb both organic and inorganic pollutants simultaneously with high adsorption. In the near future, it is crucial to direct research efforts towards making specialized modifications to these membranes, to achieve improved performance in the removal of multiple contaminants while maintaining their durability.

10. Summary

Graphene oxide–polysulfone membranes have demonstrated great potential for water purification. These membranes exhibit exceptional adsorption capacities for organic and metal ions. Recent research has enabled them to overcome their resistance to high pH and harsh chemical conditions. The fabrication of these membranes results in a superior porous structure, high compressibility, and cost-effective operation when compared to other membrane systems. Additionally, various methods have been employed to generate GO–PSF membranes, and their separation performance was tested for the removal of organic pollutants, such as methylene blue, rhodamine blue, congo red, methyl orange, tetracycline, tartrazine, rhodamine, toluene, and safranine T, as well as inorganics, including Cu(II), U(VI), Na^+, Mg^{2+}, SO_4^{2-}, As(III), Hg(II), NaCl and nitrates. The incorporation of GO into/onto PSF membranes provides a variety of pore sizes and thermal stability and enhances hydrophilicity, contributing to the adsorption capacities of the membranes. Studies have also shown that Donnan exclusion is the primary separation mechanism for GO–PSF membranes. Overall, the availability of PSF–GO derived membranes on a commercial scale is rather limited. Therefore, it is imperative that current research initiatives focus on enhancing and optimizing graphene oxide–polysulfone membranes for water purification at the industrial level.

Conflicts of interest

There are no conflicts to declare.

References

1 J. Ahmed, A. Thakur and A. Goyal, *Biological treatment of industrial wastewater*, ed. M. P. Shah, Royal Society of Chemistry, 2021.
2 C. Zamora-Ledezma, D. Negrete-Bolagay, F. Figueroa, E. Zamora-Ledezma, M. Ni, F. Alexis and V. H. Guerrero, *Environ. Technol. Innovation*, 2021, **22**, 101504.
3 M. Zubair, M. S. Roopesh and A. Ullah, *Chemosphere*, 2022, **308**, 136339.
4 M. Zubair, I. Zahara, M. Roopesh and A. Ullah, *Int. J. Biol. Macromol.*, 2023, 124446.
5 UN-Water, *Summary progress update 2021: SDG 6 – water and sanitation for all*, 2021, **https://www.unwater.org/sites/default/files/app/uploads/2021/12/SDG-6-Summary Progress-Update-2021_Version-July-2021a.pdf**.
6 P. Keramea, K. Spanoudaki, G. Zodiatis, G. Gikas and G. Sylaios, *J. Mar. Sci. Eng.*, 2021, **9**, 181.
7 N. A. Nahyoon, M. Mehdi, K. H. Thebo, N. Mahar, A. A. Memon, N. Memon and N. Hussain, *Opt. Mater.*, 2023, **135**, 113260.
8 M. M. Pendergast and E. M. Hoek, *Energy Environ. Sci.*, 2011, **4**, 1946–1971.
9 T. H. Banglani, I. Chandio, A. Ali, A. A. Memon, J. Yang, M. Kazi and K. H. Thebo, *Environ. Sci.: Water Res. Technol.*, 2024, **10**, 1061–1096.
10 A. Yusuf, A. Sodiq, A. Giwa, J. Eke, O. Pikuda, G. De Luca, J. L. Di Salvo and S. Chakraborty, *J. Cleaner Prod.*, 2020, **266**, 121867.
11 D. Li, Y. Yan and H. Wang, *Prog. Polym. Sci.*, 2016, **61**, 104–155.
12 J. Luo, W. Cao, L. Ding, Z. Zhu, Y. Wan and M. Y. Jaffrin, *Sep. Purif. Technol.*, 2012, **96**, 194–203.
13 T. Mezher, H. Fath, Z. Abbas and A. Khaled, *Desalination*, 2011, **266**, 263–273.
14 A. Ali, F. Rehman, M. Ali Khan, F. H. Memon, F. Soomro, M. Iqbal, J. Yang and K. H. Thebo, *ACS Omega*, 2022, **7**, 32410–32417.
15 S. P. Nunes, P. Z. Culfaz-Emecen, G. Z. Ramon, T. Visser, G. H. Koops, W. Jin and M. Ulbricht, *J. Membr. Sci.*, 2020, **598**, 117761.
16 P. Goh and A. Ismail, *Desalination*, 2018, **434**, 60–80.
17 M. Amirilargani, M. Sadrzadeh, E. Sudhölter and L. De Smet, *Chem. Eng. J.*, 2016, **289**, 562–582.
18 Y. Wen, J. Yuan, X. Ma, S. Wang and Y. Liu, *Environ. Chem. Lett.*, 2019, **17**, 1539–1551.

© 2024 The Author(s). Published by the Royal Society of Chemistry

Open Access Article. Published on 07 May 2024. Downloaded on 2/16/2026 7:11:56 AM. This article is licensed under a Creative Commons Attribution-NonCommercial 3.0 Unported Licence.

19 S. Bandehali, H. Sanaeepur, A. E. Amooghin, S. Shirazian and S. Ramakrishna, *Sep. Purif. Technol.*, 2021, **269**, 118731.
20 F. Abuhantash, Y. H. Abuhasheesh, H. M. Hegab, I. H. Aljundi, F. Al Marzooqi and S. W. Hasan, *J. Water Proc. Eng.*, 2023, **56**, 104310.
21 S. Karki, G. Hazarika, D. Yadav and P. G. Ingole, *Desalination*, 2023, 117200.
22 R. Majumdar, U. Mishra and B. Bhunia, *Adv. Funct. Membr. Mater. Appl*, 2022, **120**, 43–71.
23 Q. Yang, N. Adrus, F. Tomicki and M. Ulbricht, *J. Mater. Chem.*, 2011, **21**, 2783–2811.
24 M. Jiang, C. Jing, C. Lei, X. Han, Y. Wu, S. Ling, Y. Zhang, Q. Li, H. Yu and S. Liu, *Nat Sustainability*, 2024, 1–11.
25 T. M. Joseph, H. E. Al-Hazmi, B. Śniatała, A. Esmaeili and S. Habibzadeh, *Environ. Res.*, 2023, 117114.
26 M. T. Simiyu, *Investigation of the Point-of-use Water Purification Efficacy of Fabricated Diatomaceous Earth-based Filter Membranes With Static Magnetic Field*, Doctoral dissertation, University of Nairobi, 2022.
27 I. Ali, S. Z. Hasan, H. Garcia, M. K. Danquah and G. Imanova, *Chem. Eng. J.*, 2024, 149108.
28 M. Paul and S. D. Jons, *Polymer*, 2016, **103**, 417–456.
29 A. K. Ghosh and E. M. Hoek, *J. Membr. Sci.*, 2009, **336**, 140–148.
30 S. C. Mamah, P. S. Goh, A. F. Ismail, N. D. Suzaimi, L. T. Yogarathinam, Y. O. Raji and T. H. El-badawy, *J. Water Proc. Eng.*, 2021, **40**, 101835.
31 O. Dumbrava, A. Filimon and L. Marin, *Eur. Polym. J.*, 2023, 112316.
32 S. Kheirieh, M. Asghari and M. Afsari, *Rev. Chem. Eng.*, 2018, **34**, 657–693.
33 A. Khan, T. A. Sherazi, Y. Khan, S. Li, S. A. R. Naqvi and Z. Cui, *J. Membr. Sci.*, 2018, **554**, 71–82.
34 V. Kumari, P. P. Singh and S. Kaushal, *Polyhedron*, 2022, **214**, 115645.
35 S. A. E. Naser, K. O. Badmus and L. Khotseng, *Coatings*, 2023, **13**, 1456.
36 I. Mahar, F. H. Memon, J.-W. Lee, K. H. Kim, R. Ahmed, F. Soomro, F. Rehman, A. A. Memon, K. H. Thebo and K. H. Choi, *Membranes*, 2021, **11**, 869.
37 M. K. Shahzad, F. H. Memon, F. Soomro, M. Iqbal, A. Ibrar, A. A. Memon, J. H. Lim, K. H. Choi and K. H. Thebo, *J. Environ. Chem. Eng.*, 2023, **11**, 109329.
38 F. Rehman, F. Hussain Memon, S. Ullah, M. A. Jafar Mazumder, A. Al-Ahmed, F. Khan and K. Hussain Thebo, *Chem. Rec.*, 2022, **22**, e202200107.
39 I. Mahar, F. K. Mahar, N. Mahar, A. A. Memon, A. A. A. Pirzado, Z. Khatri, K. H. Thebo and A. Ali, *Chem. Eng. Res. Des.*, 2023, **191**, 462–471.
40 U. Kamran, K. Y. Rhee, S.-Y. Lee and S.-J. Park, *Chemosphere*, 2022, 135590.
41 F. Rehman, F. H. Memon, Z. Bhatti, M. Iqbal, F. Soomro, A. Ali and K. H. Thebo, *Rev. Inorg. Chem.*, 2022, **42**, 327–336.
42 A. H. Jatoi, K. H. Kim, M. A. Khan, F. H. Memon, M. Iqbal, D. Janwery, S. N. Phulpoto, A. Samantasinghar, K. H. Choi and K. H. Thebo, *RSC Adv.*, 2023, **13**, 12695–12702.
43 J. Zhou, K. Li, Z. Chen, X. Su, H. Xie, L. Yao, Y. Wu, X. Zhang, L. Chen and X. Wu, *J. Environ. Chem. Eng.*, 2023, **11**, 109840.
44 J. M. Luque-Alled, S. Leaper, A. Abdel-Karim, C. Skuse and P. Gorgojo, *J. Environ. Chem. Eng.*, 2023, **11**, 109898.
45 G. Zhao and H. Zhu, *Adv. Mater.*, 2020, **32**, 1905756.
46 W. Czepa, D. Pakulski, S. Witomska, V. Patroniak, A. Ciesielski and P. Samori, *Carbon*, 2020, **158**, 193–201.
47 K. H. Thebo, X. Qian, Q. Wei, Q. Zhang, H.-M. Cheng and W. Ren, *J. Mater. Sci. Technol.*, 2018, **34**, 1481–1486.
48 A. H. Jatoi, A. Ali, A. Nadeem, S. N. Phulpoto, M. Iqbal, A. A. Memon, J. Yang and K. H. Thebo, *New J. Chem.*, 2024, **48**, 1715–1723.
49 M.-U.-N. Khilji, A. A. Otho, R. Memon, A. Khalid, M. Kazi, A. Hyder, D. Janwery, N. A. Nahyoon, A. A. Memon and N. Memon, *Anal. Lett.*, 2023, 1–18.
50 T. Lee and B.-S. Kim, *ACS Appl. Mater. Interfaces*, 2020, **12**, 13116–13126.
51 M. Fathizadeh, W. L. Xu, F. Zhou, Y. Yoon and M. Yu, *Adv. Mater. Interfaces*, 2017, **4**, 1600918.
52 J. Zhu, J. Hou, A. Uliana, Y. Zhang, M. Tian and B. Van der Bruggen, *J. Mater. Chem. A*, 2018, **6**, 3773–3792.
53 F. A. Janjhi, D. Janwery, I. Chandio, S. Ullah, F. Rehman, A. A. Memon, J. Hakami, F. Khan, G. Boczkaj and K. H. Thebo, *ChemBioEng Rev.*, 2022, **9**, 574–590.
54 Z. Xu, J. Zhang, M. Shan, Y. Li, B. Li, J. Niu, B. Zhou and X. Qian, *J. Membr. Sci.*, 2014, **458**, 1–13.
55 A. Modi and J. Bellare, *J. Environ. Chem. Eng.*, 2019, **7**, 102944.
56 S. S. Rahman, M. Arshad, M. Zubair, M. Ghasri-Khouzani, A. Qureshi and A. Ullah, *Mater. Today Commun.*, 2020, **25**, 101633.
57 A. Alkhouzaam, H. Qiblawey and M. Khraisheh, *Membranes*, 2021, **11**, 86.
58 A. S. Lashkenari, M. T. H. Mosavian, M. Peyravi and M. Jahanshahi, *Prog. Org. Coat.*, 2019, **129**, 147–158.
59 C. Bărdacă Urducea, A. C. Nechifor, I. A. Dimulescu, O. Oprea, G. Nechifor, E. E. Totu, I. Isildak, P. C. Albu and S. G. Bungău, *Nanomaterials*, 2020, **10**, 2349.
60 N. D. Suzaimi, P. S. Goh, K. C. Wong, N. A. N. N. Malek, A. F. Ismail and J. W. Lim, *J. Membr. Sci.*, 2022, **657**, 120706.
61 L. Yu, M. Kanezashi, H. Nagasawa and T. Tsuru, *J. Membr. Sci.*, 2020, **595**, 117477.
62 M. Rezakazemi, M. Sadrzadeh and T. Matsuura, *Prog. Energy Combust. Sci.*, 2018, **66**, 1–41.
63 J.-J. Qin, S. Chen, M. H. Oo, K. A. Kekre, E. R. Cornelissen and C. J. Ruiken, *Water Sci. Technol.*, 2010, **61**, 2897–2904.
64 C. Barth, M. Goncalves, A. Pires, J. Roeder and B. Wolf, *J. Membr. Sci.*, 2000, **169**, 287–299.
65 L.-P. Cheng, D.-J. Lin and K.-C. Yang, *J. Membr. Sci.*, 2000, **172**, 157–166.
66 L. Martínez-Izquierdo, M. Malankowska, C. Téllez and J. Coronas, *J. Environ. Chem. Eng.*, 2021, **9**, 105624.
67 I. V. Maggay, M.-L. Yu, D.-M. Wang, C.-H. Chiang, Y. Chang and A. Venault, *J. Membr. Sci.*, 2022, **655**, 120597.
68 V. Mokkapati, D. Y. Koseoglu-Imer, N. Yilmaz-Deveci, I. Mijakovic and I. Koyuncu, *RSC Adv.*, 2017, **7**, 4378–4386.

© 2024 The Author(s). Published by the Royal Society of Chemistry

Open Access Article. Published on 07 May 2024. Downloaded on 2/16/2026 7:11:56 AM. This article is licensed under a Creative Commons Attribution-NonCommercial 3.0 Unported Licence.

69 A. Moosa and M. Abed, *Turk. J. Chem.*, 2021, **45**, 493–519.
70 B. C. Brodie, *Philos. Trans. R. Soc. London*, 1859, 249–259.
71 L. Staudenmaier, *Ber. Dtsch. Chem. Ges.*, 1898, **31**, 1481–1487.
72 U. Hoffmann and E. Koenig, *Z. Anorg. Allg. Chem.*, 1937, **234**, 311–336.
73 S. William, J. Hummers and R. E. Offeman, *J. Am. Chem. Soc.*, 1958, **80**, 1339.
74 K. Bansal, J. Singh and A. Dhaliwal, *IOP Conf. Ser.: Mater. Sci. Eng.*, 2022, **1225**, 012050.
75 D. C. Marcano, D. V. Kosynkin, J. M. Berlin, A. Sinitskii, Z. Sun, A. Slesarev, L. B. Alemany, W. Lu and J. M. Tour, *ACS Nano*, 2010, **4**, 4806–4814.
76 Z. Benzait, P. Chen and L. Trabzon, *Nanoscale Adv.*, 2021, **3**, 223–230.
77 R. Mukherjee, P. Bhunia and S. De, *Chem. Eng. J.*, 2016, **292**, 284–297.
78 A. M. Nasir, P. S. Goh, M. S. Abdullah, B. C. Ng and A. F. Ismail, *Chemosphere*, 2019, **232**, 96–112.
79 T. Sandle, *Sterility, Sterilisation and Sterility Assurance for Pharmaceuticals*, 2013, pp. 143–155.
80 R. Zhang, J. Tian, S. Gao and B. Van der Bruggen, *J. Mater. Chem. A*, 2020, **8**, 8831–8847.
81 A. Seidel, J. J. Waypa and M. Elimelech, *Environ. Eng. Sci.*, 2001, **18**, 105–113.
82 A. Suárez and F. A. Riera, *Desalin. Water Treat.*, 2016, **57**, 24176–24186.
83 S. Yadav, I. Ibrar, A. K. Samal, A. Altaee, S. Déon, J. Zhou and N. Ghaffour, *J. Hazard. Mater.*, 2022, **421**, 126744.
84 A. R. Nadig, N. S. Naik, M. Padaki, R. K. Pai and S. Déon, *J. Water Proc. Eng.*, 2021, **41**, 102026.
85 A. E. Yaroshchuk, *Adv. Colloid Interface Sci.*, 2000, **85**, 193–230.
86 M. Fernández de Labastida and A. Yaroshchuk, *Membranes*, 2021, **11**, 272.
87 M. Kotobuki, Q. Gu, L. Zhang and J. Wang, *Molecules*, 2021, **26**, 3331.
88 G. Liu, W. Jin and N. Xu, *Angew. Chem., Int. Ed.*, 2016, **55**, 13384–13397.
89 A. Bakshi, H. Bustamante, X. Sui and R. Joshi, *Ind. Eng. Chem. Res.*, 2021, **60**, 10917–10959.
90 L. Badrinezhad, S. Ghasemi, Y. Azizian-Kalandaragh and A. Nematollahzadeh, *Polym. Bull.*, 2018, **75**, 469–484.
91 N. A. Elessawy, J. Exley, D. S. El-Sayed, A. Toghan, S. A. Al-Hussain, M. Elzokm, A. H. Konsowa and M. Tillotson, *J. Environ. Chem. Eng.*, 2024, **12**, 112489.
92 Y. Jiang, Q. Zeng, P. Biswas and J. D. Fortner, *J. Membr. Sci.*, 2019, **581**, 453–461.
93 S. Sali, H. R. Mackey and A. A. Abdala, *Nanomaterials*, 2019, **9**, 769.
94 J. Prince, S. Bhuvana, V. Anbharasi, N. Ayyanar, K. Boodhoo and G. Singh, *Water Res.*, 2016, **103**, 311–318.
95 Y. Liu, F. Zhang, W. Zhu, D. Su, Z. Sang, X. Yan, S. Li, J. Liang and S. X. Dou, *Carbon*, 2020, **160**, 88–97.
96 A. Alammar, S.-H. Park, C. J. Williams, B. Derby and G. Szekely, *J. Membr. Sci.*, 2020, **603**, 118007.
97 T. D. Kusworo, F. Dalanta, N. Aryanti and N. H. Othman, *J. Water Proc. Eng.*, 2021, **41**, 102030.
98 A. Alkhouzaam and H. Qiblawey, *J. Membr. Sci.*, 2021, **620**, 118900.
99 A. Modi, S. K. Verma and J. Bellare, *Mater. Sci. Eng., C*, 2018, **91**, 524–540.
100 F. Chen, X. Shi, X. Chen and W. Chen, *J. Membr. Sci.*, 2018, **552**, 295–304.
101 A. Modi, S. K. Verma and J. Bellare, *Colloids Surf., B*, 2018, **167**, 457–467.
102 Y. Cai, D. Chen, N. Li, Q. Xu, H. Li, J. He and J. Lu, *J. Membr. Sci.*, 2017, **543**, 10–17.
103 B. Chakrabarty, A. Ghoshal and M. Purkait, *J. Membr. Sci.*, 2008, **325**, 427–437.
104 R. Vaghasia, B. Saini and A. Dey, *J. Mol. Liq.*, 2022, **359**, 119346.
105 Y. Wu, R. Yao, X. Zhang, B. Zhang and T. Wang, *J. Environ. Chem. Eng.*, 2021, **9**, 105164.
106 S. Zhao, Z. Wang, J. Wang and S. Wang, *J. Membr. Sci.*, 2014, **469**, 316–325.
107 S. Nasseri, S. Ebrahimi, M. Abtahi and R. Saeedi, *J. Environ. Manage.*, 2018, **205**, 174–182.
108 V. Kochkodan and N. Hilal, *Desalination*, 2015, **356**, 187–207.
109 M. Rezakazemi, A. Dashti, H. Riasat Harami and N. Hajilari, *Environ. Chem. Lett.*, 2018, **16**, 715–763.
110 Z. Wang, J. Jin, D. Hou and S. Lin, *J. Membr. Sci.*, 2016, **516**, 113–122.
111 V. Vatanpour, A. Shockravi, H. Zarrabi, Z. Nikjavan and A. Javadi, *J. Ind. Eng. Chem.*, 2015, **30**, 342–352.
112 M. J. Park, S. Phuntsho, T. He, G. M. Nisola, L. D. Tijing, X.-M. Li, G. Chen, W.-J. Chung and H. K. Shon, *J. Membr. Sci.*, 2015, **493**, 496–507.
113 M. Shaban, H. AbdAllah, L. Said, H. S. Hamdy and A. A. Khalek, *Chem. Eng. Res. Des.*, 2015, **95**, 307–316.
114 O. Abdalla, M. A. Wahab and A. Abdala, *J. Environ. Chem. Eng.*, 2020, **8**, 104269.
115 A. Romero, M. Lavin-Lopez, L. Sanchez-Silva, J. Valverde and A. Paton-Carrero, *Mater. Chem. Phys.*, 2018, **203**, 284–292.
116 S. Zinadini, A. A. Zinatizadeh, M. Rahimi, V. Vatanpour and H. Zangeneh, *J. Membr. Sci.*, 2014, **453**, 292–301.
117 M. L. Pedersen, T. R. Jensen, S. V. Kucheryavskiy and M. E. Simonsen, *J. Photochem. Photobiol., A*, 2018, **366**, 162–170.
118 S. Kim, D. E. Heath and S. E. Kentish, *Desalination*, 2023, **548**, 116277.
119 L. Mérai, Á. Deák, I. Dékány and L. Janovák, *Adv. Colloid Interface Sci.*, 2022, **303**, 102657.
120 P. G. Torres-Valenzuela, J. Álvarez-Sánchez, G. E. Dévora-Isiordia, M. M. Armendáriz-Ontiveros, M. del Rosario Martínez-Macias, S. Pérez-Sicairos, R. G. Sánchez-Duarte and G. A. Fimbres Weihs, *Polym. Bull.*, 2023, **80**, 6285–6306.
121 L. Song, *J. Membr. Sci.*, 1998, **139**, 183–200.
122 M. S. Ramasamy, A. Rahaman and B. Kim, *Ceram. Int.*, 2021, **47**, 11010–11021.

© 2024 The Author(s). Published by the Royal Society of Chemistry

Open Access Article. Published on 07 May 2024. Downloaded on 2/16/2026 7:11:56 AM. This article is licensed under a Creative Commons Attribution-NonCommercial 3.0 Unported Licence.

123 T. Virtanen, G. Rudolph, A. Lopatina, B. Al-Rudainy, H. Schagerlöf, L. Puro, M. Kallioinen and F. Lipnizki, *Sci. Rep.*, 2020, **10**, 3427.
124 A. Kovtun, M. Zambianchi, C. Bettini, A. Liscio, M. Gazzano, F. Corticelli, E. Treossi, M. L. Navacchia, V. Palermo and M. Melucci, *Nanoscale*, 2019, **11**, 22780–22787.
125 N. Lekena, T. A. Makhetha and R. M. Moutloali, *J. Environ. Chem. Eng.*, 2023, **11**(5), 110883.
126 Q. Gao, L. Duan, Y. Jia, H. Zhang, J. Liu and W. Yang, *Membranes*, 2023, **13**, 837.
127 L. Jaber, I. W. Almanassra, A. AbuShawish, A. Chatla, I. Ihsanullah, M. M. Ali, Y. Manawi, A. Shanableh and M. A. Atieh, *J. Membr. Sci.*, 2024, **691**, 122259.
128 V. Vatanpour, S. S. Madaeni, R. Moradian, S. Zinadini and B. Astinchap, *J. Membr. Sci.*, 2011, **375**, 284–294.
129 D. Rana and T. Matsuura, *Chem. Rev.*, 2010, **110**, 2448–2471.
130 A. Razmjou, J. Mansouri and V. Chen, *J. Membr. Sci.*, 2011, **378**, 73–84.
131 X. Chen, E. Deng, D. Park, B. A. Pfeifer, N. Dai and H. Lin, *ACS Appl. Mater. Interfaces*, 2020, **12**, 48179–48187.
132 J. Liang, Y. Tan, Y. Yu, Y. Hu and C. Liao, *Polym. Adv. Technol.*, 2023, **34**, 1575–1584.
133 M. Hu and B. Mi, *Environ. Sci. Technol.*, 2013, **47**, 3715–3723.
134 A. Rossi, M. Zannotti, M. Cuccioloni, M. Minicucci, L. Petetta, M. Angeletti and R. Giovannetti, *Nanomaterials*, 2021, **11**, 1733.
135 X. Cao, C. Ma, J. Zhao, H. Guo, Y. Dai, Z. Wang and B. Xing, *Sci. Total Environ.*, 2019, **679**, 270–278.
136 F. A. A. Ali, J. Alam, A. K. Shukla, M. Alhoshan, M. A. Ansari, W. A. Al-Masry, S. Rehman and M. Alam, *React. Funct. Polym.*, 2019, **140**, 136–147.
137 N. S. Suhalim, N. Kasim, E. Mahmoudi, I. J. Shamsudin, N. L.-A. Jamari and F. Mohamed Zuki, *Membranes*, 2023, **13**, 602.
138 L. Yu, W. Zhou, Y. Li, Q. Zhou, H. Xu, B. Gao and Z. Wang, *ACS Sustain. Chem. Eng.*, 2019, **7**, 8724–8734.
139 Y. T. Chung, E. Mahmoudi, A. W. Mohammad, A. Benamor, D. Johnson and N. Hilal, *Desalination*, 2017, **402**, 123–132.
140 R. Huang, S. Zhang, W. Zhang and X. Yang, *IET Collaborative Intelligent Manufacturing*, 2021, **3**, 281–289.
141 S. Balta, A. Sotto, P. Luis, L. Benea, B. Van der Bruggen and J. Kim, *J. Membr. Sci.*, 2012, **389**, 155–161.
142 R. Rajakumaran, M. Kumar and R. Chetty, *Desalination*, 2020, **495**, 114673.
143 V. Mokkapati, D. Y. K. Imer, N. Yilmaz, V. Ozguz and I. Koyuncu, *RSC Adv.*, 2015, **5**, 71011–71021.
144 M. Safarpour, A. Khataee and V. Vatanpour, *Ind. Eng. Chem. Res.*, 2014, **53**, 13370–13382.
145 Y. T. Chung, L. Y. Ng and A. W. Mohammad, *J. Ind. Eng. Chem.*, 2014, **20**, 1549–1557.
146 M. J. Hajipour, K. M. Fromm, A. A. Ashkarran, D. J. de Aberasturi, I. R. de Larramendi, T. Rojo, V. Serpooshan, W. J. Parak and M. Mahmoudi, *Trends Biotechnol.*, 2012, **30**, 499–511.
147 A. Sirelkhatim, S. Mahmud, A. Seeni, N. H. M. Kaus, L. C. Ann, S. K. M. Bakhori, H. Hasan and D. Mohamad, *Nano-Micro Lett.*, 2015, **7**, 219–242.
148 A. Akbar, M. B. Sadiq, I. Ali, N. Muhammad, Z. Rehman, M. N. Khan, J. Muhammad, S. A. Khan, F. U. Rehman and A. K. Anal, *Biocatal. Agric. Biotechnol.*, 2019, **17**, 36–42.
149 G. Fan, J. Ge, H.-Y. Kim, B. Ding, S. S. Al-Deyab, M. El-Newehy and J. Yu, *RSC Adv.*, 2015, **5**, 64318–64325.
150 Q. Huang, Z. Ding, H. Lu, M. Geng, J. Liu, M. Meng, Z. Liu, Y. Liu and J. Pan, *Sep. Purif. Technol.*, 2023, **325**, 124694.
151 A. Pattammattel, M. Puglia, S. Chakraborty, I. K. Deshapriya, P. K. Dutta and C. V. Kumar, *Langmuir*, 2013, **29**, 15643–15654.
152 G. S. Prihandana, T. Sriani, A. D. Muthi'ah, A. Machmudah, M. Mahardika and N. Miki, *Nanomaterials*, 2022, **12**, 388.
153 S. S. Hosseini, E. Bringas, N. R. Tan, I. Ortiz, M. Ghahramani and M. A. A. Shahmirzadi, *J. Water Proc. Eng.*, 2016, **9**, 78–110.
154 O. Abdalla, A. Rehman, A. Nabeeh, M. A. Wahab, A. Abdel-Wahab and A. Abdala, *Membranes*, 2023, **13**, 678.
155 V. K. Thakur and S. I. Voicu, *Carbohydr. Polym.*, 2016, **146**, 148–165.
156 J. Liu, C. Zhao, Z. Zhang, J. Liao, Y. Liu, X. Cao, J. Yang, Y. Yang and N. Liu, *Chem. Eng. J.*, 2016, **288**, 505–515.
157 L. Ghasemi-Mobarakeh, M. P. Prabhakaran, L. Tian, E. Shamirzaei-Jeshvaghani, L. Dehghani and S. Ramakrishna, *World J. Stem Cell.*, 2015, **7**, 728.
158 K. I. John, M. O. Omorogie, A. A. Bayode, A. T. Adeleye and B. Helmreich, *Chem. Pap.*, 2023, **77**, 657–676.
159 M. Kasbaji, M. Mennani, A. Boussetta, N. Grimi, F. J. Barba, M. Mbarki and A. Moubarik, *Sep. Sci. Technol.*, 2023, **58**, 221–240.
160 T. D. Kusworo, H. Susanto, N. Aryanti, N. Rokhati, I. N. Widiasa, H. Al-Aziz, D. P. Utomo, D. Masithoh and A. C. Kumoro, *J. Environ. Chem. Eng.*, 2021, **9**, 105066.
161 R. Hu, G. Zhao, Y. He and H. Zhu, *Desalination*, 2020, **477**, 114271.
162 X. Luo, Q. Yan, C. Wang, C. Luo, N. Zhou and C. Jian, *Int. J. Environ. Res. Public Health*, 2015, **12**, 11975–11987.
163 S. J. Ajeel, A. A. Beddai and A. M. N. Almohaisen, *Mater. Today: Proc.*, 2022, **51**, 289–297.
164 A. T. Yasir, A. Benamor, M. Ba-Abbad and A. H. Hawari, *J. Water Proc. Eng.*, 2024, **60**, 105095.
165 Y. Tamer, M. D. Özeren and H. Berber, *J. Polym. Environ.*, 2021, **29**, 4000–4016.
166 J. Ma, M. Zhang, M. Ji, L. Zhang, Z. Qin, Y. Zhang, L. Gao and T. Jiao, *Int. J. Biol. Macromol.*, 2021, **193**, 2221–2231.
167 Y. Tamer, A. Koşucu and H. Berber, *Int. J. Biol. Macromol.*, 2022, **219**, 273–289.
168 R. Castaldo, R. Avolio, M. Cocca, M. E. Errico, M. Lavorgna, J. Šalplachta, C. Santillo and G. Gentile, *Chem. Eng. J.*, 2022, **430**, 133162.
169 Z. Yang, X. Liu, X. Liu, J. Wu, X. Zhu, Z. Bai and Z. Yu, *Colloids Surf., B*, 2021, **200**, 111605.
170 L. Lentz, D. A. Mayer, M. Dogenski and S. R. S. Ferreira, *Mater. Chem. Phys.*, 2022, **283**, 125981.

Open Access Article. Published on 07 May 2024. Downloaded on 2/16/2026 7:11:56 AM. This article is licensed under a Creative Commons Attribution-NonCommercial 3.0 Unported Licence.

171 B. Chen, Y. Li, M. Li, M. Cui, W. Xu, L. Li, Y. Sun, M. Wang, Y. Zhang and K. Chen, *Microporous Mesoporous Mater.*, 2021, **328**, 111457.
172 Y. Tamer and H. Berber, *J. Macromol. Sci., Part A: Pure Appl.Chem.*, 2022, 1–14.
173 N. Jahan, H. Roy, A. H. Reaz, S. Arshi, E. Rahman, S. H. Firoz and M. S. Islam, *Case Stud. Chem. Environ. Eng.*, 2022, **6**, 100239.
174 I. H. Alsohaimi, M. S. Alhumaimess, A. A. Alqadami, G. T. Alshammari, R. F. Al-Olaimi, A. A. Abdeltawab, M. Y. El-Sayed and H. M. Hassan, *Inorg. Chem. Commun.*, 2023, **147**, 110261.
175 G. Natesan and K. Rajappan, *Environ. Sci. Pollut. Res.*, 2023, **30**, 42658–42678.
176 D. R. Rout and H. M. Jena, *Environ. Res.*, 2022, **214**, 114044.
177 S. J. Kim, S. H. Ko, K. H. Kang and J. Han, *Nat. Nanotechnol.*, 2010, **5**, 297–301.
178 C. Shivalingam, L. Mohan, D. Ganapathy, R. Shanmugam, S. Pitchiah, R. Ramadoss and A. K. Sundramoorthy, *Curr. Anal. Chem.*, 2022, **18**, 989–998.
179 H. Wang, W. Wang, L. Wang, B. Zhao, Z. Zhang, X. Xia, H. Yang, Y. Xue and N. Chang, *Chem. Eng. J.*, 2018, **334**, 2068–2078.
180 K. Y. Wang and T. S. Chung, *AIChE J.*, 2006, **52**, 1363–1377.
181 T.-S. Chung, X. Li, R. C. Ong, Q. Ge, H. Wang and G. Han, *Curr. Opin. Chem. Eng.*, 2012, **1**, 246–257.
182 T. Y. Cath, S. Gormly, E. G. Beaudry, M. T. Flynn, V. D. Adams and A. E. Childress, *J. Membr. Sci.*, 2005, **257**, 85–98.
183 R. W. Holloway, A. E. Childress, K. E. Dennett and T. Y. Cath, *Water Res.*, 2007, **41**, 4005–4014.
184 H. Salehi, A. Shakeri and S. R. Razavi, *ACS ES&T Water*, 2022, **2**, 508–517.
185 L. Chekli, S. Phuntsho, H. K. Shon, S. Vigneswaran, J. Kandasamy and A. Chanan, *Desalin. Water Treat.*, 2012, **43**, 167–184.
186 S. Phuntsho, H. K. Shon, T. Majeed, I. El Saliby, S. Vigneswaran, J. Kandasamy, S. Hong and S. Lee, *Environ. Sci. Technol.*, 2012, **46**, 4567–4575.
187 M. Ganj, M. Asadollahi, S. A. Mousavi, D. Bastani and F. Aghaeifard, *J. Polym. Res.*, 2019, **26**, 1–19.
188 M. R. S. Emami, M. K. Amiri and S. P. G. Zaferani, *Korean J. Chem. Eng.*, 2021, **38**, 316–325.
189 P. Babuji, S. Thirumalaisamy, K. Duraisamy and G. Periyasamy, *Water*, 2023, **15**, 2532.
190 K. Tulugan, P. Tian, X. Li, W. Zhao, X. Zhang and Y. Zhao, *J. Eng. Res.*, 2024, DOI: **10.1016/j.jer.2024.01.001**.
191 S. Poolachira and S. Velmurugan, *Environ. Res.*, 2022, **210**, 112924.
192 F. Zhu, L. Kong, M. He, D. Fang, X. Hu and X. Peng, *Water Res.*, 2023, **243**, 120355.
193 A. Maher, M. Sadeghi and A. Moheb, *Desalination*, 2014, **352**, 166–173.
194 S. Dhara, A. Sontakke, N. Samanta, M. K. Purkait and R. V. Uppaluri, *Sep. Purif. Technol.*, 2024, **341**, 126894.
195 P. Sherugar, N. S. Naik, M. Padaki, V. Nayak, A. Gangadharan, A. R. Nadig and S. Déon, *Chemosphere*, 2021, **275**, 130024.
196 N. Politaeva, A. Yakovlev, E. Yakovleva, V. Chelysheva, K. Tarantseva, S. Efremova, L. Mukhametova and S. Ilyashenko, *Water*, 2022, **14**, 1430.
197 M. Nasir, Y. Purnama Utami, N. Faaizatunnisa, L. Rohmawati, E. Suebah, A. Taufiq and E. S. Sazali, *J. Water Environ. Nanotechnol.*, 2023, **8**, 241–253.
198 I. Akin and E. Zor, *J. Environ. Chem. Eng.*, 2024, 111976.
199 M. Khajouei, M. Najafi, S. A. Jafari and M. Latifi, *Micromachines*, 2023, **14**, 128.
200 S. Amiri, V. Vatanpour and T. He, *Chemosphere*, 2023, **322**, 138159.
201 A. M. Alosaimi, *Polymers*, 2021, **13**, 2792.
202 R. Mondal and S. De, *Environ. Technol. Innovation*, 2022, **26**, 102300.
203 Y. Liu, *Ceram. Int.*, 2018, **44**, 18571–18577.
204 X. Hao, S. Yang, E. Tao and Y. Li, *J. Hazard. Mater.*, 2022, **424**, 127680.
205 C. Ding and H. Qi, *Membranes*, 2023, **13**, 536.
206 S. Velusamy, A. Roy, S. Sundaram and T. Kumar Mallick, *Chem. Rec.*, 2021, **21**, 1570–1610.
207 M. Verma, I. Lee, J. Oh, V. Kumar and H. Kim, *Chemosphere*, 2022, **287**, 132385.
208 Y. Kuang, Z. Zhang and D. Wu, *Sci. Total Environ.*, 2022, **806**, 151258.
209 K. Li, T. Xiong, J. Liao, Y. Lei, Y. Zhang and W. Zhu, *Chem. Eng. J.*, 2022, **433**, 134449.
210 N. Liu, H. Liang, W. Tian, C. Li, Q. Gao, N. Wang, R. Guo and Z. Mo, *Colloids Surf., A*, 2022, **649**, 129367.
211 S. Dhara, A. D. Sontakke, N. S. Samanta, R. V. S. Uppaluri and M. K. Purkait, *Sep. Purif. Technol.*, 2024, 126894.
212 A. V. Talyzin, G. Mercier, A. Klechikov, M. Hedenström, D. Johnels, D. Wei, D. Cotton, A. Opitz and E. Moons, *Carbon*, 2017, **115**, 430–440.
213 A. S. Kuzenkova, A. Y. Romanchuk, A. L. Trigub, K. I. Maslakov, A. V. Egorov, L. Amidani, C. Kittrell, K. O. Kvashnina, J. M. Tour and A. V. Talyzin, *Carbon*, 2020, **158**, 291–302.
214 K. Erickson, R. Erni, Z. Lee, N. Alem, W. Gannett and A. Zettl, *Adv. Mater.*, 2010, **22**, 4467–4472.
215 H.-P. Boehm, A. Clauss, G. Fischer and U. Hofmann, *Proceedings of the Fifth Conference on Carbon*, 1962.
216 A. G. Klechikov, G. Mercier, P. Merino, S. Blanco, C. Merino and A. V. Talyzin, *Microporous Mesoporous Mater.*, 2015, **210**, 46–51.
217 A. V. Talyzin, T. Szabó, I. Dékány, F. Langenhorst, P. S. Sokolov and V. L. Solozhenko, *J. Phys. Chem. C*, 2009, **113**, 11279–11284.
218 A. Klechikov, J. Sun, G. Hu, M. Zheng, T. Wågberg and A. V. Talyzin, *Microporous Mesoporous Mater.*, 2017, **250**, 27–34.
219 N. Boulanger, A. S. Kuzenkova, A. Iakunkov, A. Y. Romanchuk, A. L. Trigub, A. V. Egorov, S. Bauters, L. Amidani, M. Retegan and K. O. Kvashnina, *ACS Appl. Mater. Interfaces*, 2020, **12**, 45122–45135.

© 2024 The Author(s). Published by the Royal Society of Chemistry

Open Access Article. Published on 07 May 2024. Downloaded on 2/16/2026 7:11:56 AM.
This article is licensed under a Creative Commons Attribution-NonCommercial 3.0 Unported Licence.

220 K. S. Kim, Y. Zhao, H. Jang, S. Y. Lee, J. M. Kim, K. S. Kim, J.-H. Ahn, P. Kim, J.-Y. Choi and B. H. Hong, *Nature*, 2009, **457**, 706–710.
221 Y. Huang, L. Taylor, X. Chen and N. Ayres, *J. Polym. Sci., Part A: Polym. Chem.*, 2013, **51**, 5230–5238.
222 Y. Zhao, J. Li, L. Zhao, S. Zhang, Y. Huang, X. Wu and X. Wang, *Chem. Eng. J.*, 2014, **235**, 275–283.
223 S. Yang, J. Hu, C. Chen, D. Shao and X. Wang, *Environ. Sci. Technol.*, 2011, **45**, 3621–3627.
224 H. Chen, D. Shao, J. Li and X. Wang, *Chem. Eng. J.*, 2014, **254**, 623–634.
225 J.-b. Huo, G. Yu and J. Wang, *Chemosphere*, 2021, **278**, 130492.
226 C. Ursino, R. Castro-Muñoz, E. Drioli, L. Gzara, M. H. Albeirutty and A. Figoli, *Membranes*, 2018, **8**, 18.
227 K. Golzar, S. Amjad-Iranagh, M. Amani and H. Modarress, *J. Membr. Sci.*, 2014, **451**, 117–134.
228 O. Hölck, M. Böhning, M. Heuchel, M. R. Siegert and D. Hofmann, *J. Membr. Sci.*, 2013, **428**, 523–532.
229 J. Yang, Z. Shen, J. He and Y. Li, *J. Membr. Sci.*, 2021, **630**, 119331.
230 C. L. Ritt, J. R. Werber, A. Deshmukh and M. Elimelech, *Environ. Sci. Technol.*, 2019, **53**, 6214–6224.
231 Z. Zhang, L. Huang, Y. Wang, K. Yang, Y. Du, Y. Wang, M. J. Kipper, L. A. Belfiore and J. Tang, *Phys. Chem. Chem. Phys.*, 2020, **22**, 6032–6057.
232 J. Muscatello, F. Jaeger, O. K. Matar and E. A. Müller, *ACS Appl. Mater. Interfaces*, 2016, **8**, 12330–12336.
233 B. Chen, H. Jiang, X. Liu and X. Hu, *J. Phys. Chem. C*, 2017, **121**, 1321–1328.
234 H. Dai, Z. Xu and X. Yang, *J. Phys. Chem. C*, 2016, **120**, 22585–22596.
235 H. Zhang, B. Liu, H. T. Kieu, M. S. Wu, K. Zhou and A. W.-K. Law, *J. Membr. Sci.*, 2018, **558**, 34–44.
236 Y. Kang, M. Obaid, J. Jang, M.-H. Ham and I. S. Kim, *Chemosphere*, 2018, **207**, 581–589.
237 Y. Lou, G. Liu, S. Liu, J. Shen and W. Jin, *Appl. Surf. Sci.*, 2014, **307**, 631–637.
238 J. Shen, G. Liu, K. Huang, Z. Chu, W. Jin and N. Xu, *ACS Nano*, 2016, **10**, 3398–3409.
239 M. Kumar, N. Sreedhar, N. Thomas, M. Mavukkandy, R. A. Ismail, T. M. Aminabhavi and H. A. Arafat, *Chem. Eng. J.*, 2022, **433**, 133526.